The Pennsylvania State University

The Graduate School

College of Engineering

THE EFFECTS OF CELL MORPHOLOGY ON NANOPARTICLE UPTAKE AND UPTAKE AT THE LEADING EDGE IN MC3T3 CELLS

A Thesis in

Bioengineering

by

Harvey S. Li

Submitted in Partial Fulfillment
of the Requirements
for the Degree of

Master of Science

May 2018

The thesis of Harvey S. Li was review and approved* by the following:

Justin L. Brown
Associate Professor of Biomedical Engineering
Thesis Adviser

William Hancock
Professor of Biomedical Engineering
Chair of the Intercollege Graduate Program in Bioengineering

Xiaojun Lian
Assistant Professor of Biomedical Engineering

* Signatures are on file in the Graduate School.

ABSTRACT

When using the correct material coupled with drugs and specific surface ligands, nanoparticles can have enhanced targeted drug delivery properties. Currently, scientists can alter the size, shape, material, and surface properties among other factors in order to change the characteristics of the nanoparticles and how the body reacts to them[1]. While much research has been done looking at how varying the properties of nanoparticles affect nanoparticle uptake, little research has been done to see how varying cell properties affect nanoparticle uptake. Additionally, it is known that the extracellular matrix of tumor tissue is different than that of healthy tissue. The differences in ECM organization causes the tumor cells to take on certain patterns, which may affect nanoparticle and drug uptake. The aims of this project are twofold: first, I will compare the rate of nanoparticle uptake at the leading edge to that at the trailing edge, then, I would like to see how cell morphology affects nanoparticle uptake. The results from these experiments indicate that there is a difference in nanoparticle uptake in elongated and non-elongated cells. The leading edge of a cell also appears to contain more nanoparticles than the trailing edge of a cell; however, this is not dependent on cellular elongation.

TABLE OF CONTENTS

LIST OF FIGURES

ACKNOWLEDGEMENTS

I would like to thank Dr. Justin Brown for letting me join his lab just after my freshman year. I would also like to thank Dr. Pouria Fattahi, who mentored me on this project, Dr. Brittany Banik, who taught me about cell culture, and Dr. Dan Bowers, who assisted me with live-cell imaging techniques. I am also grateful to all of other lab members and friends that I have met in these past five years for keeping me grounded. Finally, I would like to thank my family for constantly reminding me not to procrastinate on my thesis.

Chapter 1

Background

The medical field is constantly evolving to better fit the needs of patients. A relatively new field in medicine is drug delivery. This area of study focuses on finding the optimal method for transporting the drug to a target, which can be an organ, a type of cell, or even a sequence of DNA, among other things.

A History of Drug Delivery

The history of drug delivery can be traced back thousands of years ago to the first uses of herbal remedies to treat diseases[2]. However, these remedies hold no scientific merit. A modern history of drug delivery can be separated into three generations: Generation I (1950-1980), Generation II (1981-2010), and Generation III (2010-2040)[3]. Generation I was characterized by only a basic understanding of drug release. At this time, no technology existed that could control the release rate of a drug; these drugs are often known as "rapid-release" drugs because of this. Patients were simply told how much and often to take a drug (e.g. one pill twice a day), and most delivery methods were either oral or transdermal delivery[3]. The concept of controlling the release rate of a drug started in the mid-1960s, when Dr. Judah Folkman discovered that anesthetic gasses can diffuse through silicone rubber tubing at a specific rate[4]. He hypothesized that a constant rate of drug delivery could be achieved using silicone tubing to control the release of the drug[4].

The idea of a constant rate of drug delivery, or zero-order delivery, marked the transition from Generation I to Generation II of drug delivery. A controlled delivery eliminated the need for constant dosages, which decreased the frequent changes in drug concentration within the body as well as the side effects associated with these fluctuations[2]. In the late 1960s, Alejandro Zaffaroni, after being inspired by Dr. Folkman's work, founded ALZA, a company that focused on producing drugs that utilize controlled drug delivery. By the 1980s, ALZA had developed a method for controlled drug release in the GI tract called OROS, which stands for Osmotic Release Oral System. OROS worked by utilizing a rate-controlling membrane, which controlled the rate at which water entered the drug capsule through osmosis. As water entered the capsule, the building osmotic pressure would then push the active drug out of an opening in the capsule, resulting in a constant rate of drug release[2,4]. ALZA also developed a controlled release system for implantable devices called DUROS. This system differs from OROS in that the rate-controlling membrane is used to control the release of the drug rather than the intake of water. One common device to utilize this technology is the intrauterine device (IUD); the rate controlling membrane allowed for the device to release the hormone progesterone at a constant rate[4].

During Generation II, there was also a push for the development of drug delivery systems that can "sense" the surrounding environmental factors. These systems would then release the drug based on changes in pH or glucose levels[3]. In the 1970s, Folkman and Langer showed that hydrophobic polymer matrices could be used to control the release of biomolecular drugs[4]. Their findings caught the attention of many other researchers, and started an interest in developing smart polymers and hydrogels. Research on the pharmacologic uses of nanoparticles as drug delivery vehicles also began during this generation in the 1970s[4]. The development of smart

polymers and hydrogels merged with the interest in nanoparticle drug delivery, creating nanoparticles with various types of material properties. This new but rapidly growing field of research combined material sciences, biology, and engineering. When using the correct material coupled with drugs and specific surface ligands, nanoparticles can have enhanced targeted drug delivery properties.

These research trends continued past the turn of the century, and into the 2010s where research currently stands. These years also mark the transition into the third generation of drug delivery systems. New developments in nanomedicine and modular drug delivery systems are a hallmark of this generation[3].

Nanoparticles

Jörg Kreuter may have been the first to use the term "nanoparticle" in 1976 when describing the drug-containing micelles developed by Dr. Birrenbach[3,5,6]. Birrenbach pioneered the idea of attaching drugs and antigens to these nanoparticles to aid in drug delivery systems. His research showed that fragile biological molecules, such as proteins, could be stably contained within the micelle nanoparticle and released when they enter the body[5]. Modern nanoparticle research builds upon the foundation established by Birrenbach; now, in addition to creating drug-containing micelles, scientists can alter the size, shape, material, and surface properties among other factors in order to change the characteristics of the nanoparticles and how the body reacts to them[1].

Nanoparticle material plays an important role in how the nanoparticles behave *in vivo*. Birrenbach utilized amphipathic lipids to encase the drugs or biological molecules in self

assembling micelles. Micelle-like nanoparticles and their drug delivery abilities are still being studied today. In addition to micelle-like nanoparticles, scientists can now make nanoparticles out of various polymers. These polymeric nanoparticles were initially made of nonbiodegradable polymers, such as poly(methyl methacrylate) (PMMA), polystyrene, and polyacrylates. Since these polymers are not biodegradable, they must be excreted from the body so that they do not reach a toxic concentration within the body. Due to the risks of toxicity, there has been a shift towards biodegradable polymers, such as poly(lactide) (PLA) and poly (ε-caprolactone) (PCL), as well as other natural polymers[7]. Polymeric nanoparticles are not hollow so the drugs and biological molecules must be adhered to the surface of the nanoparticle rather than being contained on the inside of the nanoparticle. This paper will focus mainly on polymeric nanoparticles.

One of the most widely studied nanoparticle factors is size. Depending on the fabrication method and material, the size of the nanoparticles can be controlled[7]. The size of a nanoparticle can range anywhere from 1 nm to slightly over 1 μm. This property plays a large role in the cellular uptake of nanoparticles. Some cells will not take in nanoparticles if they are too large or too small; Caco-2 and Madin-Darby cells were found to only take in nanoparticles smaller than 200 nm in diameter. Additionally, nanoparticles in the range of 100-200 nm show the most potential in crossing the gastrointestinal barrier and blood-brain barrier[8]. Current research also shows that nanoparticles in the 10-100 nm range should be used for cancer therapy due to the enhanced permeability and retention (EPR) effect. This effect stems from the non-functioning lymph system in tumors; the blood vessels in the tumor leak macromolecules (or in this case, nanoparticles) into the tumor where they accumulate[1]. One must also consider how size affects the cellular uptake method; cells utilize receptor-medicated endocytosis to consume

nanoparticles in the 100-200 nm range, whereas larger nanoparticles are consumed through phagocytosis. The size of the nanoparticle can also affect toxicity, targeting, circulation, opsonization, and degredation[7].

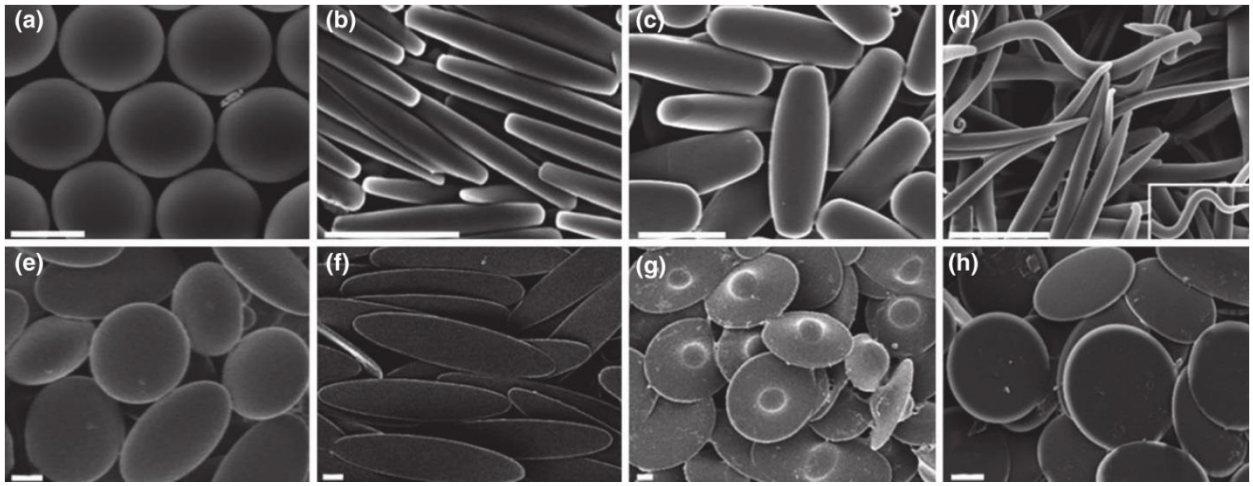

Figure 1. Nanoparticle morphology. (a) Spheres, (b) rectangular disks, (c) rods, (d) worms, (e) oblate ellipses, (f) elliptical disks, (g) unidentified flying objects (UFOs), and (h) circular disks (scale bars: 2um). Image taken from Champion et. al. (Ref. 25)

Another important factor regarding the efficacy of nanoparticles is the geometry of the nanoparticle. While nanoparticles are typically spherical, they can also be shaped like rectangular disks, rods, worms, oblate ellipses, elliptical disks, UFOs, and circular disks (Figure 1)[7]. The shape of the nanoparticle will affect cellular interactions. Researchers have found that the cellular uptake rate of the nanoparticles in the 1 – 10 μm range is determined by the angle formed by the line defining the particle curvature at the point of contact between the particle and the cell, and the membrane normal at the point of contact (Figure 2)[9]. There is a critical angle of about 45° where any angle larger than this will cause the cell to not consume the nanoparticle, and instead the cell will spread over the particle[9]. The morphology will also affect how the nanoparticles travel in the blood stream and how they will dissolve, if they are biodegradable[7]. Currently, it is difficult to make any hard conclusions about the effects of nanoparticle

morphology on cellular interactions, other than that the contact angle affects cellular uptake rate, as it is still an active area of research.

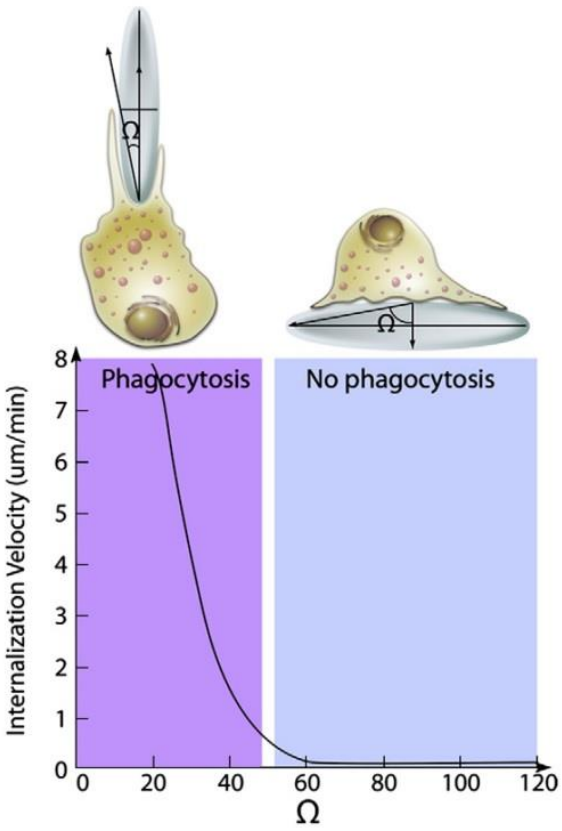

Figure 2. Internalization velocity vs. angle formed by particle curvature line and the membrane normal at the point of contact. Image taken from Sahay et. al. (Ref. 9)

Nanoparticle surface chemistry is critical in determining how the nanoparticle will interact with cells. A common practice is to alter the surface charge of the nanoparticle. Slight positive or negative charges can be imparted on the nanoparticles by treating them with certain chemicals; for example, carboxymethyl chitosan will impart a negative charge and chitosan hydrochloride will impart a positive charge on the nanoparticles[10]. The nanoparticles must also be sterically stabilized so that they do not undergo self-self interactions and coagulate[1]. Imparting charges on the nanoparticles affect how they will act within the body. The surface of cells, especially those that compose the blood vessel endothelium, are negatively charged.

Anionic nanoparticles will be diverted from these cells[1]. The charge can also determine how nanoparticles enter the cell. Negatively charged particles utilize a caveolae mediated mechanism to move into the cell, whereas neutral and positively charged particles enter through non-clathrin and non-caveolae mechanisms[11].

The surface chemistry also determines what cells the nanoparticles will target. Targeting ligands can be bound to the surface of the nanoparticle. These ligands can include peptides and antibodies that target the surface receptors of a specific cell type[1]. A common target is cancer, since many cancers have an increased expression of certain surface receptors. Conversely, ligands can be added to the nanoparticle to conceal it from certain cells and the immune system. These are known as stealth ligands. Stealth ligands allow the nanoparticles to circulate through the blood for longer periods of time, as they are less likely to be removed by the immune system[7,12].

Cellular Uptake Mechanisms

Cells consume particles through endocytosis. Endocytosis can be separated into two main categories: phagocytosis and pinocytosis. Phagocytosis translates to “cell eating” and is used to take in larger particles, bacteria, or even other cells. Phagocytosis is only present in phagocytic cells. Pinocytosis translates to “cell drinking” and is used to take in fluids and solutes; this method of intake is present in all cells. Nanoparticles are typically consumed via pinocytosis. Pinocytosis can be classified into subcategories based on the proteins involved with the entry of the particles (Figure 3)[9]. The previously stated nanoparticle characteristics (material, morphology, surface chemistry, etc.) can all affect which pathway the nanoparticle is ultimately

taken up by. Most nanoparticles enter the cell through either clathrin mediated endocytosis or caveolae mediated endocytosis[13–15].

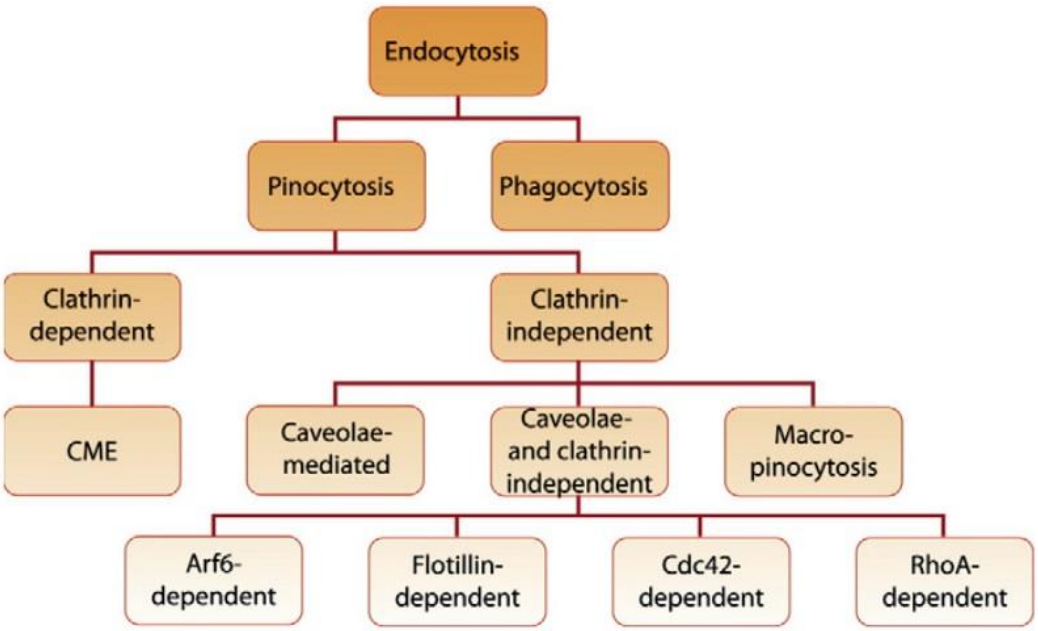

Figure 3. Methods of endocytosis. Image taken from Sahay et. al. (Ref. 9)

Clathrin mediated endocytosis (CME) is the most common method of cellular uptake for non-phagocytic cells[9]. This route is often used for cholesterol or iron uptake, so low density lipoprotein receptors and transferrin receptors are used as markers to identify CME[14]. CME occurs when transmembrane receptors and their ligands gather in clathrin coated pits on the plasma membrane. The pits then deepen and are pinched off by dynamin, a GTPase. This process creates clathrin coated vesicles (CCVs). The CCVs, which contain the receptors and bound ligands, are then uncoated, becoming endosomes, and attached to the actin cytoskeleton where they are moved to wherever the cell directs them[9,14].

Some nanoparticles such as poly(ethylene glycol) (PEG), polylactide (PLA), and poly(lactic-co-glycolic acid) (PLGA) have been observed to enter cells through CME. However,

the method of cellular intake seems to depend more on cell type than nanoparticle type. Polarized Madin-Darby canine kidney (MDCK) epithelial cells took in PEG and PLA nanoparticles via CME regardless of nanoparticle surface charge. In non-polarized HeLa cells, positively charged nanoparticles solely utilized CME whereas negatively charged nanoparticles were able to utilize both CME and caveolae-mediated endocytosis. PLGA nanoparticles were observed to use CME to enter vascular smooth muscle cells (VSMCs), but used both clathrin-independent and caveolae-independent endocytosis when introduced to rat corneal epithelial cells[9].

Caveolae mediated endocytosis is another popular cellular entry pathway used by nanoparticles. Much like how clathrin mediated endocytosis is defined by the use of the protein clathrin, caveolae mediated endocytosis utilizes the membrane proteins caveolin-1, caveolin-2, and caveolin-3. The caveolin protein generates flask-shaped pits, known as caveolae[9,14,15]. Caveolae mediated endocytosis is less selective than clathrin mediated endocytosis; a variety of molecules can bind to the caveolae and be taken into the cell. Additionally, the caveolae mediated pathway can avoid lysosomal digestion. However, because of the lax selectivity and lysosome evasion, viruses and bacteria can take advantage of this pathway to infect the cell. At the same time, nanoparticles delivering fragile biological molecules like protein and DNA would want to utilize this pathway to avoid lysosomal degradation[9].

Drugs such as DOXIL and Abraxane already exploit caveolae mediated endocytosis to deliver drugs to cancer cells. Studies have shown that poly(ethyleneoxide)-b-poly(methacrylic acid) (PEO-b-PMA) core-cross-linked polymeric micelles (cl-micelles) can specifically target cancer cells and utilize the caveolae mediated endocytic pathway[9]. Current research is trying to identify targetable proteins in caveolae. Aminopeptidase P (APP) was identified as one such

target in the caveolae of lung endothelium tumors. When bound with APP antibodies, gold nanoparticles were able to accumulate in the caveolae of cancerous lung endothelial cells[9,16].

There are clathrin and caveolae independent pathways, like Arf6-dependent and Flotillin-dependent endocytosis, but these pathways are not yet well characterized. While there are some nanoparticles that utilize these pathways, very few have been observed to do so[9,14,15,17]. More research will have to be done in this area to elucidate how these pathways may affect drug delivery.

Recently, studies in mechanobiology have been done showing that cell surface mechanics affect cellular endocytosis[18,19]. Substrate stiffness is known to affect cellular membrane tension, which affects nanoparticle uptake. Cells on softer substrates with lower membrane tensions are observed to intake more nanoparticles than cells on stiffer substrates with higher membrane tensions[19]. Within the human body, the extracellular matrix (ECM) on which cells reside can vary in stiffness and density. Cancerous tissues are known to have different ECM properties at various stages of development, and have cells in distinct patterns[18–21]. Thus, it is important to study how cell morphology can affect nanoparticle uptake; this can be used to aid in the uptake of nanoparticles in diseased tissues.

Chapter 2

Methods

Cell Culture

Cell culture began with obtaining a mouse-derived osteoblast precursor cell line, known as MC3T3 cells, from Pouria. These cells were seeded onto a 145 mm x 20 mm Greiner CELLSTAR® dish and fed with 20 ml of alpha-modified minimum essential medium (α-MEM). 1% volume/volume penicillin/streptomycin from Lonza and 10% fetal bovine serum (FBS) from Atlanta Biologicals is added to the α-MEM. The media was changed every two days. All procedures done with live cells were done in a NUAIRE LABGARD ES Class II, Type A2, Biological Safety Cabinet. When cells would reach 80% confluency or greater, they would be passaged onto another dish. Cell dishes were stored in a Nuaire Autoflow IR Direct Heat CO_2 Incubator at 37 °C and 5% CO_2.

Passaging is when the population of cells in a cell culture dish becomes too large so a portion of those cells are seeded onto a new dish and the rest are either used in an experiment or discarded. When passaging cells, the media is first aspirated from the dish. Cells are then washed with 5 ml of 1x phosphate-buffered saline (PBS). 1x PBS is made by dissolving 20 g of NaCl (VWR), 0.5 g of KCl (Sigma-Aldrich), 6.8 G of $Na_2HPO_4 \bullet 7H_2O$ (VWR), and 0.6 g KH_2PO_4 (VWR) in 100 ml of distilled-deionized water (ddH_2O). The pH is adjusted to 7.4 using HCl (EMD-Millipore) and a S220 SevenCompact™ pH meter. ddH_2O is then added until the volume reaches 250 ml. The resulting solution is 10x PBS, which is then diluted to 1x PBS by

adding ddH_2O. Washing the cells with 1x PBS removes the serum from the cells that was in the media. This is done so that the remaining serum will not inactivate the trypsin used in the next step. 5 ml of trypsin-EDTA from Mediatech Inc. is added to the dish, which is then incubated for five minutes. Trypsin breaks the cells' focal adhesions to the plate so that the cells are no longer attached to the surface of the plate. After five minutes, cells were observed under a Nikon® Eclipse TE300 microscope. If the cells are free-floating in the trypsin, 5 mL of α-MEM is added. If the cells remain attached to the dish, they are placed back into the incubator until they are free-floating. Since trypsin is toxic to cells, the α-MEM is added to neutralize the trypsin. All 10 ml of the cells in trypsin- α-MEM solution is pipetted into a 15 ml CELLSTAR® tube from Greiner Bio One using a Gilson Inc. MACROMAN™ pipette. The tube is then centrifuged in a Thermo Scientific Heraeus Multifuge X1 Centrifuge, using another 15 ml CELLSTAR® tube filled with 10 ml of water as a counterweight, at 500 RPM for 5 minutes. After centrifugation, the trypsin- α-MEM solution is aspirated from the CELLSTAR® tube and 10 ml of pure α-MEM is added to the tube. The α-MEM is pipetted in and out a few times to break up the clump of cells at the bottom of the tube. Once the cells are even dispersed throughout the media, 1/4 - 1/2 of the media is added to a new 145 mm x 20 mm Greiner CELLSTAR® dish. The amount of the media added to the dish is dependent upon how soon the cells will be needed; using a larger portion of the media will allow the cells to reach confluency sooner. When a portion of the cells and media have been added to the new dish, the remaining cells can be aspirated and the tube disposed of. α-MEM is then added to the new dish until the total volume of α-MEM in the dish is 20 ml. The new dish is then placed in the incubator.

Cover Slip Preparation

22 mm x 22 mm glass cover slips were obtained from VWR. They were sprayed with pure ethanol and wiped clean with a KIMTECH Kimwipe. The cleaned cover slips were then coated with a thin layer of 20% poly(methyl methacrylate) (PMMA) (Sigma-Aldrich) in nitromethane (Sigma-Aldrich) (weight/volume) by using a Laurrell Technologies spin coater (Model Ws-400BZ-6NPP/Lite). Spin coating is the process of placing a small amount of polymer solution on a cover slip and spinning the cover slip at high speeds to spread the polymer in an even coat around the cover slip. 100 µl of 20% PMMA in nitromethane was used for each slide and the slides were spun for 10 seconds at 5000 RPM. The PMMA creates a suitable environment for cell growth on the cover slips.

After spin coating, half of the cover slips was designated as "film" and the other half was designated as "scratched." The film cover slips were complete after the spin coating process. The scratched cover slips had to be scratched with sandpaper to create grooves in the PMMA for cells to adhere to. This causes the cells to have an elongated morphology. To scratch the cover slips, the cover slips were pressed PMMA-side down onto P2000 grit silicon carbide sandpaper. The cover slip was then dragged along the width of the paper once (Figure 4). Since P2000 grit sandpaper utilizes particles with an average diameter of 10.3 µm, the thickness of the scratched lines can be assumed to be approximately 10.3 µm.

Once five film and five scratched cover slips have been made, cells can be seeded onto them. The cover slip seeding protocol follows the cell passage protocol with the exception of a few steps. The cover slips are placed into two Grenier Bio-One CELLSTAR 6-well plates, with one cover slip per well and the PMMA side facing up. All scratched slides are placed on the top row of the 6-well plates and the film slides are placed on the row below the scratched slides. The

cover slips and 6-well plates are then placed under UV light for five minutes to kill any possible contaminants on them. This can be done while the cells are being centrifuged. After the cells are centrifuged and are dispersed in the new media, 10 µl of the cells are taken from the tube and placed onto a Fisher Scientific hemacytometer where they are counted. This will give an estimate of the concentration of cells in the tube. Once the concentration is known, approximately 15,000 cells are pipetted from the tube and dropped onto a cover slip. This is repeated for each cover slip. 2 ml of α-MEM is added to each well and then the 6-well plates are placed in the incubator. The rest of the cell passage protocol is then completed with the remaining cells.

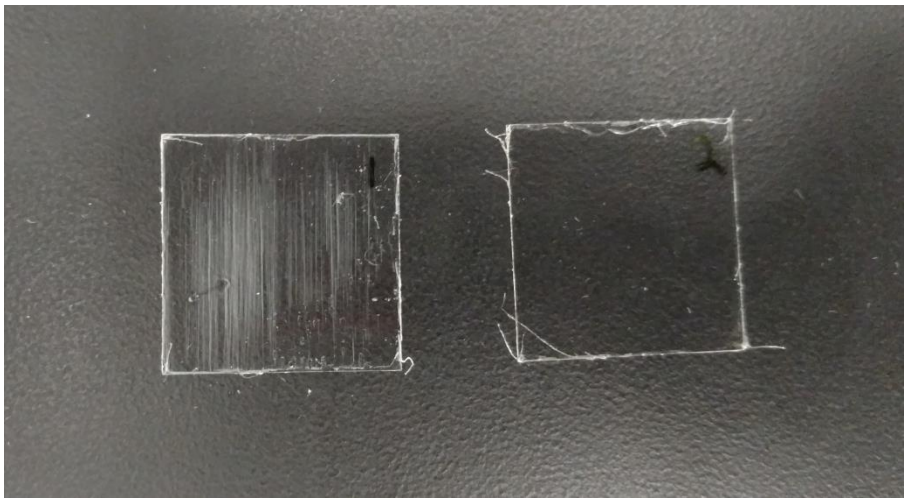

Figure 4. Scratched cover slip (left) vs. film cover slip (right)

Nanoparticle Uptake

In order to calculate the rate of nanoparticle uptake, fluorescent polystyrene (PS) nanoparticles were introduced to the cells at different time points. The time points were 24, 12, 8, 4, and 1 hour before they are fixed for immunostaining. A nanoparticle-media solution was

created. Nanoparticles were added to α-MEM at a ratio of 10 µl of nanoparticles to 1 ml of α-MEM. Each well in a 6-well plate requires 2 ml of media so 200 µl of nanoparticles was mixed with 20 ml of α-MEM in a 50 ml CELLSTAR® tube for the 10 cover slips. The tube was inverted one to two times to evenly disperse the nanoparticles throughout the media. 24 hours before the cells are fixed for immunostaining, the α-MEM in two wells are aspirated (one containing a scratched slide and the other containing a film slide). The aspirated media is replaced with 2 ml per well of the nanoparticle-media solution. The 6-well plate is then placed back in the incubator. This process is repeated at 12, 8, 4, and 1 hour before the cells undergo immunostaining.

Immunofluorescence

Immunostaining requires fixation buffer (FB) and permeabilization buffer (PB). 25 ml of fixation buffer is made by mixing 2.5 ml of 3.7% - 4% paraformaldehyde (VWR) in 22.5 ml of 1x PBS. 50 ml of permeabilization buffer is made by adding 500 µl of 0.1% Triton X-100 and dissolving 1.5 g of 3% bovine serum albumin (BSA) (VWR) in 50 ml of 1x PBS. Cytoskeletal stabilization buffer (CSB) is also used; this is made by dissolving 0.146 g of NaCl, 0.151 g of piperazine-N,N′-bis(2-ethanesulfonic acid) (PIPES), 0.012 g of $MgCl_2$, 0.019 g of EGTA, and 5.134 g of sucrose in 250 µl of 0.5% Triton X100 and 50 ml of DI water. Protease and phosphatase inhibitors are added at 100 µl per 10 ml of solution. The pH of the solution is then adjusted to 6.8 using HCl or NaOH. Following the preparation of FB, PB, and CSB, the nanoparticle-α-MEM solution is aspirated from all of the wells and they are all washed with 1x PBS. After five minutes, the 1x PBS is aspirated and 2ml of ice cold CSB is added to each well and left for one

minute at room temperature before being aspirated. 2 ml of FB is added to each well and left to incubate at room temperature for 15 minutes. The FB is aspirated and the cover slips are then washed again with 1x PBS, but this time they are washed three times for 5 minutes each. 2 ml of PB is then added to each well and is left to incubate at room temperature for 45 minutes. During this time, the primary antibody solution can be prepared. The primary antibody is mixed in a 1:500 ratio of antibody to PB. The primary antibody used binds to γ-tubulin and is a polyclonal antibody derived from rabbits (abcam). γ-tubulin is used as a marker to define the leading edge of a cell; when the slides are viewed under a microscope, the leading edge can be defined. From this point in the protocol, only 1 ml of solution will be used per well. 20 µl of primary antibody is mixed with 10 ml of PB. After the 45 minute incubation period, the PB is aspirated from the wells and 1 ml of primary antibody solution is added per well. This is allowed to incubate for one hour. The secondary antibody solution can be prepared during this time. The secondary antibody binds to the primary antibody and is fluorescent; this allows the protein that the primary antibody tagged to be seen under a fluorescent microscope. Goat anti-rabbit IgG (H+L), DyLight® 650 conjugated (Thermo Scientific) is used as the secondary antibody and is mixed in a 1:1000 ratio of antibody to PB. 10 µl of primary antibody is mixed with 10 ml of PB. Following the one hour incubation period for the primary antibody, the PB and primary antibody are aspirated from the wells and the cover slips are washed with 1x PBS three times for five minutes each time. Then the secondary antibody solution is added 1 ml to each well. The secondary antibody is incubated for 45 minutes at room temperature in the dark since the secondary antibody is light sensitive. The 6-well plates are wrapped in aluminum foil to prevent light from entering. During the incubation period, a solution of DAPI, phalloidin 488 (Biotium), and PB is prepared. DAPI stains the A-T regions in DNA, whereas phalloidin stains F-actin.

This allows us to see the nucleus and cytoskeleton respectively. Phalloidin and DAPI are added to PB at a concentration of 1:1000 and 1:5000 respectively. For 10 ml of solution, 10 µl of phalloidin and 2 µl of DAPI are added to 10 ml of PB. After the secondary antibody incubation period, the PB and secondary antibody are aspirated from the wells and the cover slips are washed with 1x PBS three times for five minutes each time. Then 1 ml of the phalloidin-DAPI-PB solution is added to the wells. The cover slips are left to incubate one last time at room temperature for 30 minutes in the dark. After the 30 minute incubation period, the phalloidin-DAPI-PB solution is aspirated and the cover slips are washed with 1x PBS three times for five minutes each time. The cover slips are then mounted onto VWR 75 mm x 25 mm microscope slides. Approximately 30 µl of Fluoromount-G™ (Electron Microscopy Sciences) mounting media is dropped onto the slide and the cover slip is placed PMMA side down onto the mounting media. Each slide can fit two cover slips. Label each cover slip and let them rest until the mounting media dries at room temperature in the dark. Once the mounting media has dried, clear nail polish is applied to the edges of the cover slides to prevent them from moving when under the microscope. The slides can now be imaged using a Leica® DM5500B.

Actin/Myosin Inhibition

Y-27632 can be used to inhibit F-actin polymerization and myosin II. Specifically, Y-27632 inhibits rho-associated protein kinase (ROCK) pathways. This ends up inhibiting F-actin and myosin II, which are downstream of the inhibition site. F-actin and myosin II are essential for the formation stress fibers; without stress fibers, there would be no cell migration, cellular

contractility, or mechanotransduction. Thus, this test can indicate whether the difference in nanoparticle uptake is dependent on stress fibers or not.

Y-27632 was obtained from Cytoskeleton Inc. The inhibitor in each vial was reconstituted by adding 100 µl of ddH_2O to each vial. Y-27632 should act within 30 minutes of application, but to be safe, it was added 2 hours before the introduction of any nanoparticles (see Cover Slip Preparation and Nanoparticle Uptake). To use the inhibitor, 10 µl of inhibitor solution is added to the cover slips for every 1 ml of media. Two hours after the application of the inhibitor, nanoparticles can be added. However, since the inhibitor is reversible (i.e. the effects of the inhibitor are reversed once the inhibitor is removed from the media), the inhibitor-containing media cannot be aspirated and replaced with nanoparticle-containing media. Instead of creating a nanoparticle-media mixture, nanoparticles are added directly to each well. 1 µl of nanoparticle is added per 1 ml of media; thus, 2 µl of nanoparticles are added to each well. Following the addition of nanoparticles at the specific time points, the immunostaining protocol can be performed.

Microcontact Printing

The next step of the experiment is to create a more controllable way for the cells to elongate. This is done through microcontact printing (µCP). µCP allows users to create a tiny area, large enough for a single cell to adhere to, in a specific shape. To start µCP, a stamp of polydimethylsiloxane (PDMS) is made. In this case, I wanted rectangles with aspect ratios of 1, 5, and 8. I obtained a PDMS stamp with the shapes I wanted from Pouria. A solution of 1% pluronic acid F-127 is made by mixing pluronic acid with ddH_2O and letting it sit for one hour at

room temperature. Each stamp will get 10 ml of the pluronic solution. Fibronectin solution made by mixing fibronectin and ddH_2O in a ratio of 25 µg of fibronectin to 1 ml of ddH_2O. Once the two solutions are made, the PDMS stamp is cleaned with ethanol spray and dried using compressed air. The cleaned stamp is then coated with O_2 plasma, using a Plasma Cleaner PDC-001 (Harrick Plasma). The coating process is set for about 45 seconds per stamp. O_2 plasma coating causes the surface of the stamp to become very hydrophilic. This allows the stamp to easily absorb any solutions put on it. Finally, the PDMS stamp is placed under a UV light for 5 minutes to disinfect it. Once the PDMS stamp has been disinfected, enough fibronectin is added to the stamp to completely cover the stamping face. The stamp is left to absorb the fibronectin for 1.5 hours.

22 mm x 22 mm glass cover slips are prepared for stamping by being spin-coated with 100 µl of PDMS. The PDMS is made beforehand by mixing SYLGARD® 184 Silicone Elastomer Base with SYLGARD® 184 Silicone Elastomer Curing Agent (Dow Corning) in a 10:1 ratio respectively. They are then coated with O_2 plasma for 30 seconds and disinfected under UV light for 5 minutes. After the stamp has absorbed the fibronectin, the remaining excess fibronectin is aspirated off. ddH_2O is added and then blown off with compressed air. The stamp is then placed lightly on a glass cover slip. A tweezer is used to gently press down the perimeter of the stamp before lightly pressing in the center of the stamp. The stamp is left to sit on the cover slip for one minute. It is then carefully removed using tweezers. Since the stamp had previously absorbed fibronectin to its surface, it will leave fibronectin prints of the desired shape on the surface of the cover slip. This process is repeated for each cover slip. 10 ml of pluronic is then added onto the cover slips using a filtered syringe and left on the cover slips for ten minutes. Pluronic F-127 now coats the entire surface of the cover slip apart from the few

islands of fibronectin. Pluronic prevents cell focal adhesions from being formed so when cells are eventually added to the cover slip, they will be forced to attach to the islands of fibronectin. The islands of fibronectin are small enough to allow for just a single cell to attach in a specific shape (Figure 5). After ten minutes, the pluronic can be aspirated off and 10 ml of 1x PBS is added onto the cover slips before being aspirated immediately. 1x PBS is added again to the cover slips, but this time left for five minutes before being aspirated. This process is repeated two more times, each time aspirating the 1x PBS after five minutes. To clean the stamps, the stamps are placed in a 50 ml tube with ddH_2O and sealed with parafilm (Bemis). A Fisher Scientific Ultrasonic Bath sonicator is used to heat the tube at 60 ℃ for 20 minutes to remove any residual fibronectin from the stamp. This is repeated a second time, but the ddH_2O is removed and replaced with ethanol.

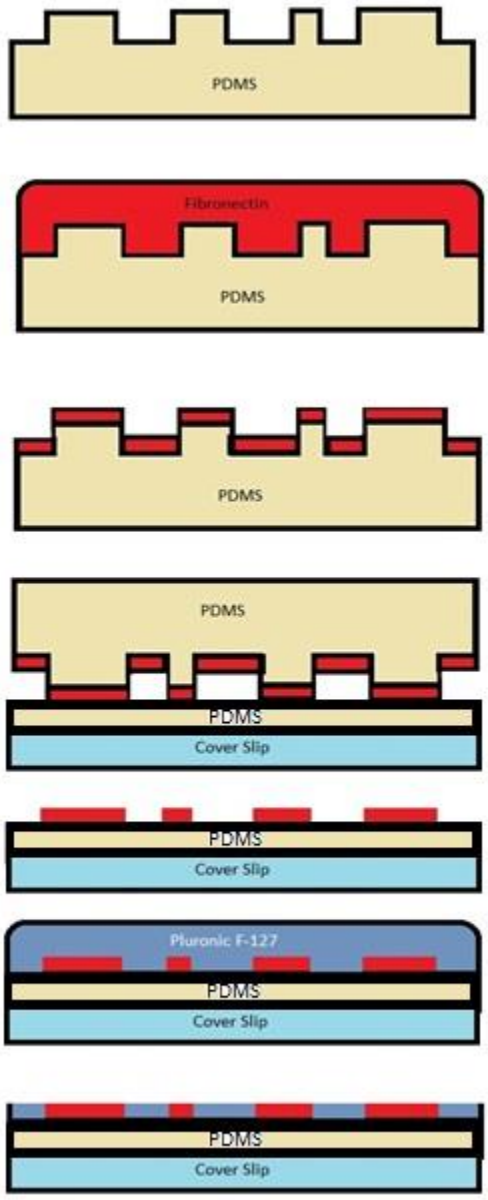

Figure 5. Microcontact printing protocol

Following this process, the cover slips are ready to be seeded with cells. To seed cells onto the cover slips, the cell passage protocol until after the cells have been centrifuged. Once the cells have been centrifuged and are dispersed in the new media, 10 µl of the cells are taken from the tube and placed onto a Fisher Scientific hemacytometer to be counted. The cover slips are placed into a Grenier Bio-One CELLSTAR 6-well plate, with one cover slip per well and the

stamped side facing up. 2 ml of the cell-α-MEM mixture is pipetted onto each cover slip and the cover slips are placed in the incubator. Depending on how high the cell count was, the cover slips are checked every 5-10 minutes for cell adhesion (a higher cell count requires less time). Once the cells are seen to be attaching to the fibronectin spots, the cell-α-MEM mixture is aspirated to avoid multiple cells adhering to a single fibronectin stamp. 2 ml of α-MEM is added to each well after the cell-α-MEM mixture is aspirated.

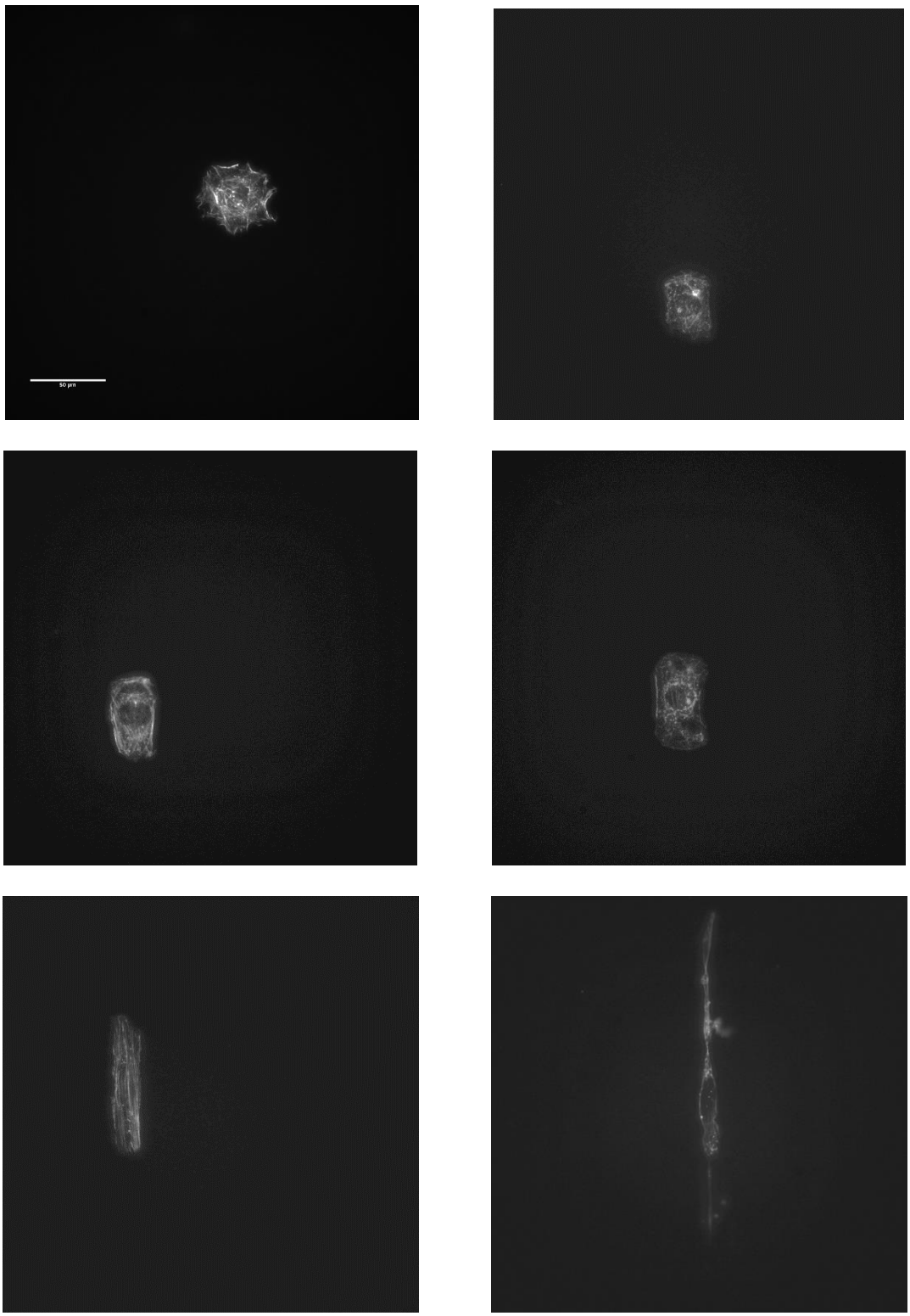

Figure 6. Stamped cells of varying aspect ratios. Top left: circle, top right 1:1, middle left 1:1.5, middle right 1:2, bottom left 1:4, bottom right 1:8. Scale bar in top left image is 50 µm. All images were taken at 40x

Live Cell Imaging

Following microcontact printing experiments, live cell imaging of stamped cells was used to compare nanoparticle uptake patterns in elongated and non-elongated cells. A 35mm dish with a hole in the bottom first needs to be prepared by heating a cork borer on a hot plate, then pressing the hot cork borer through the bottom of the 35mm polystyrene dish. A razor blade is then used to smooth the edges around the hole. Once the hole is smooth, drops of UV curing glue are placed around the rim of the hole. A 22x22mm glass coverslip is then placed onto the glue and rotated to create a clear watertight bond. The glue is then cured by placing the dish with the coverslip under a UV light for at least two minutes. The custom dish is then sterilized in the biological safety hood by putting it under UV light for at least five minutes. The microcontact printing protocol is then performed as previously described, using the glued coverslip as the coverslip for printing.

One hour prior to starting the timelapse, the 40x objective is heated with the stage heater (BioPTECH) to prevent the lens from expanding and losing focus during the timelapse. The α-MEM is removed from the custom dish and replaced with 2 ml of warmed imaging media. The custom dish is then moved to the pre-warmed microscope stage. The objective is lowered into the imaging media and then 2 ml of warmed mineral oil (AMRESCO) is added to prevent evaporation. The mineral oil must be added gently to prevent mixing of the water and oil. Once the selected cell is in focus, the correct exposure is set using the live view on the computer. The time-lapse was set to take a picture in five minute intervals for 145 cycles. This gave a time-lapse of approximately 12 hours.

Chapter 3

Results and Discussion

Film vs Line Fluorescent Microscopy

The immunofluorescence protocol suggests using CSB when immunostaining, but CSB may cause nanoparticles to leak out of the cell. Initially, the step involving CSB was skipped for this reason. However, multiple experiments were done without CSB and in all of those experiments, the γ-tubulin stain did not show up clearly. Repeating the experiments with CSB revealed that using CSB will clearly show the γ-tubulin stain. All subsequent stains were done with CSB and the results only utilize data from experiments with CSB.

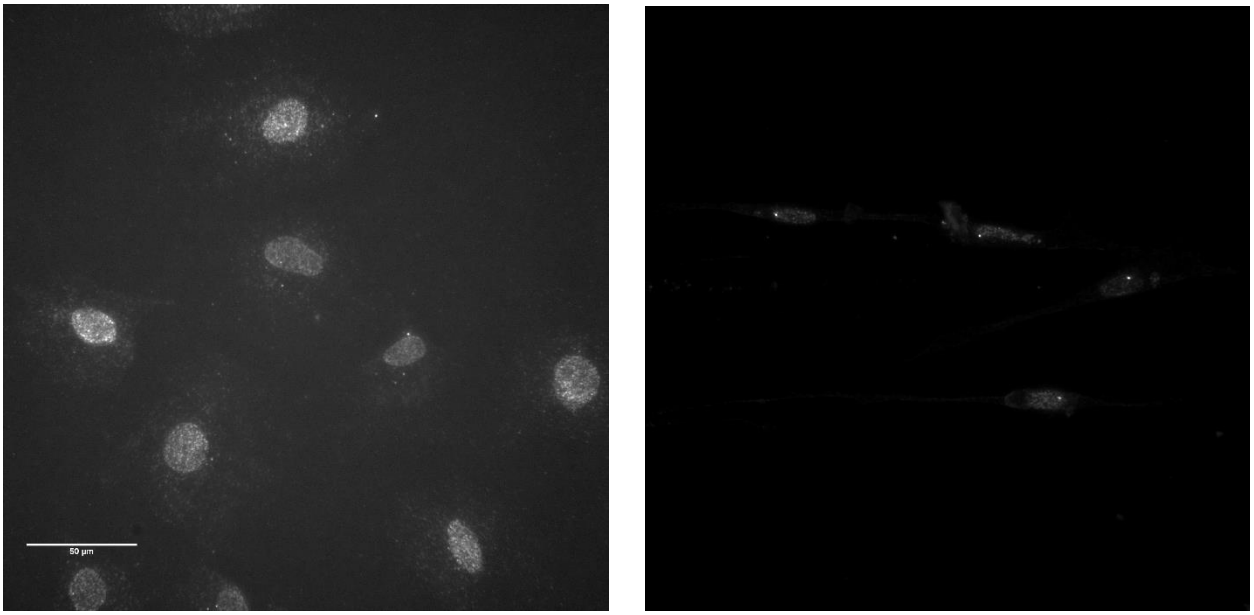

Figure 7. The image on the left shows the γ-tubulin stain when no CSB is used, and the image on the right shows the γ-tubulin stain when CSB is used. The bright magenta dot, which shows γ-tubulin, is clearly seen on the right, but not on the left. The scale bar on the left image is 50 µm. Both images were taken at 40x

Following immunostaining, the slides were imaged on a Leica® DM5500B microscope. In order to have comparable nanoparticle intensities, the exposure time for the nanoparticles was kept at 400 ns for all images. Since the intensities of the other cellular components (nucleus,

actin, and γ-tubulin) were not being measured, their exposures were adjusted to create the most visible image. Separate fluorescent images of the nuclei, actin, γ-tubulin, and nanoparticles were taken.

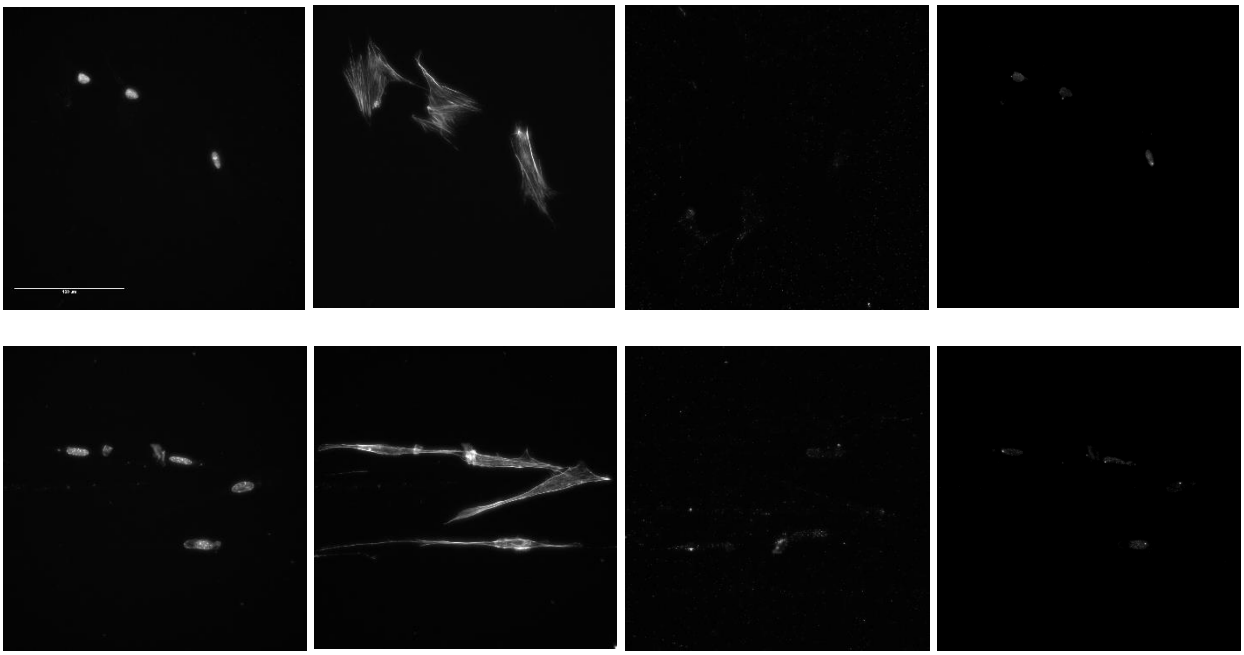

Figure 8. (Top) From left to right, these are images of the nucleus, actin, nanoparticles, and γ-tubulin of a cell on a 24 hour film substrate. (Bottom) From left to right, these are images of the nucleus, actin, nanoparticles, and γ-tubulin of a cell on a 12 hour line substrate. The scale bar in the top left image is 100 µm. All images were taken at 40x

A CellProfiler pipeline was then made to quantify the images taken from the microscope. This pipeline consisted of loading the nuclei, actin, and nanoparticle fluorescent images. All the nuclei in the image was first identified and the nuclei area was measured. Then the actin image was used to find the outline of each cell; the cell area was also calculated. Finally, CellProfiler measured the intensity of the nanoparticles in each cell. Outliers were calculated and removed using Grubbs' Test. Data from the 1, 4, and 8 hour time points were not used since there was no detectable trend in these data. This may be due to cells needing time to sense their surroundings and conform to them before any mechanotransduction signaling occurs.

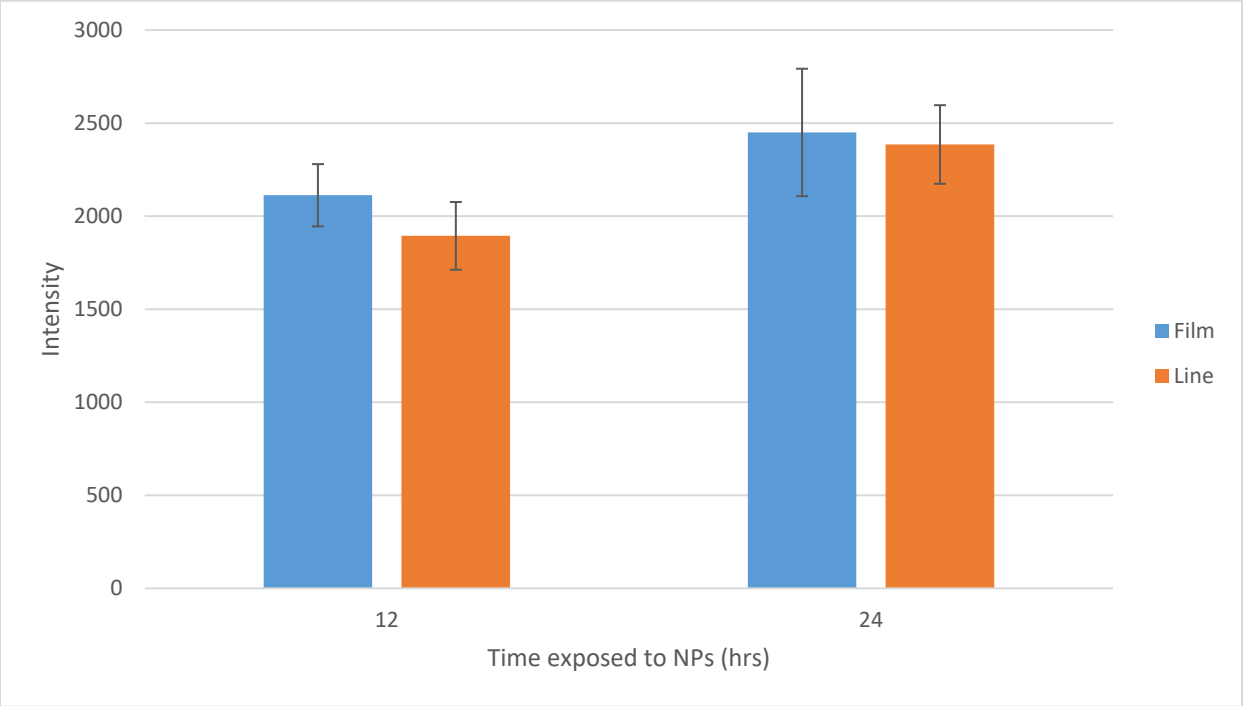

Figure 9. Cells on film have a slightly higher overall intensity than cells on a line substrate. The difference in intensity between line and film is not statistically significant for either time point. N = 20 for the line substrate and N = 14 for the film substrate at 12 hours. N = 10 for both the line and film substrates at 24 hours. All error bars in this paper show the standard error of the mean

For the 12 and 24 hour time points, there is a general upwards trend, indicating that with more time, cells will intake more nanoparticles. This is to be expected based on previous experiments. The data also shows that the cells on PMMA film have a slightly higher intake than the cells on the grooved, or line, PMMA substrate. This data seems to follow the data in the Huang et. al. paper, which found reduced nanoparticle uptake for cells on a nanofiber substrate[18]. While Huang et. al. used a nanofiber substrate, the grooves used in this experiment can be thought of as inverted nanofibers. This is also supported by the idea that cells with a higher membrane tension will intake less nanoparticles than cells with a lower membrane tension[19,21]. For the 12 hour time point, the nanoparticle uptake for cells on the grooved substrate is lower by about 10%. For the 24 hour time point, the grooved substrate cellular uptake is still lower than that of the film substrate, but only by about 2.6%. Using an unpaired t-test, the intensity

difference between the film and grooved substrate for both the 12 and 24 hour time points were deemed to be not statistically significant. The P values were 0.4018 and 0.8696 respectively.

Another trend seen in the data is that the intensity of the cells on the grooved substrate increased more than that of the cells on the film from 12 to 24 hours. As previously stated, the difference between the grooved and film substrate intensities decreased from 10% to 2.6%. This is most likely due to the cells becoming saturated with nanoparticles. Previous studies have found cells to become saturated anywhere from 7 hours to 25 hours[22,23].

However, if the intensity is normalized with respect to cell area, a different pattern emerges.

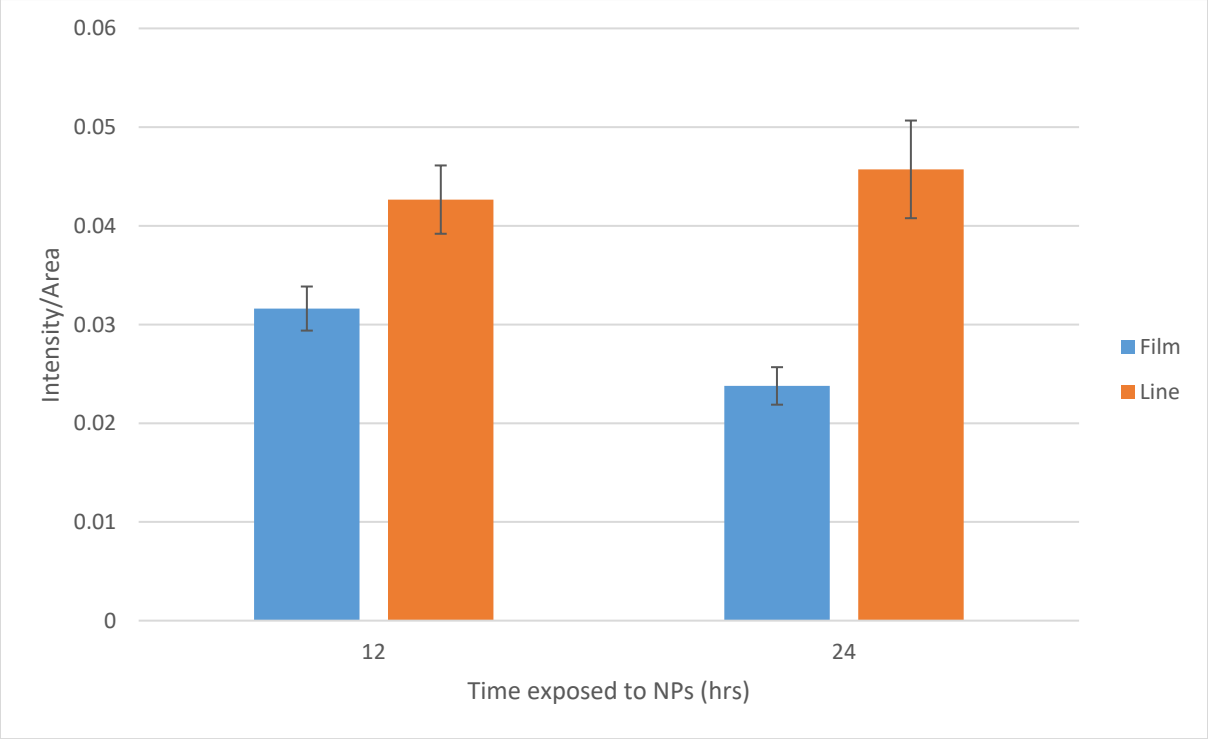

Figure 10. Cells on a film substrate have a lower intensity per unit area than cells on a line substrate. The difference is statistically significant at both time points.

The grooved substrate cells have a higher intensity with respect to area compared to the film substrate. Additionally, the intensity/area value for the film substrate decreases from 12 to 24

hours; this is due to the cells spreading and increasing their area as opposed to a decrease in nanoparticle intake since we saw an increase in intensity. Since the cells on the grooved substrate are confined in their morphology, they cannot spread and thus have a much smaller area than the cells on the flat substrate. Using an unpaired t-test, the difference in intensity/area for both the 12 hour and 24 hour time points is considered to be statistically significant with P values of 0.0156 and 0.0003 respectively.

Next, the fluorescence intensity of the leading edge was compared to that of the trailing edge for cells on film and line substrates. This was done using ImageJ. Using the γ-tubulin images, a line was drawn through the midpoint of the nucleus and the γ-tubulin using the straight line tool. This line was then copied to the actin image, where it was extended from one edge of the cell to the other. The resulting line was bisected with a second line, which now separates the leading edge from the trailing edge. The leading edge of the cell was then identified based on the "direction" of the γ-tubulin and manually outlined using the polygon selection tool. The outlines were then copied and superimposed on the corresponding nanoparticle image. ImageJ then measured the intensity and area of the region within the outlines. This was done for all cells completely within the frame. The process is repeated for the trailing edge, but outlining the trailing edge instead of the leading edge. All of the intensity values were normalized with respect to area since the area of the leading edge did not necessarily equal the area of the trailing edge. Again, outliers were identified and removed using Grubbs' test and only the 12 and 24 hour time points are used.

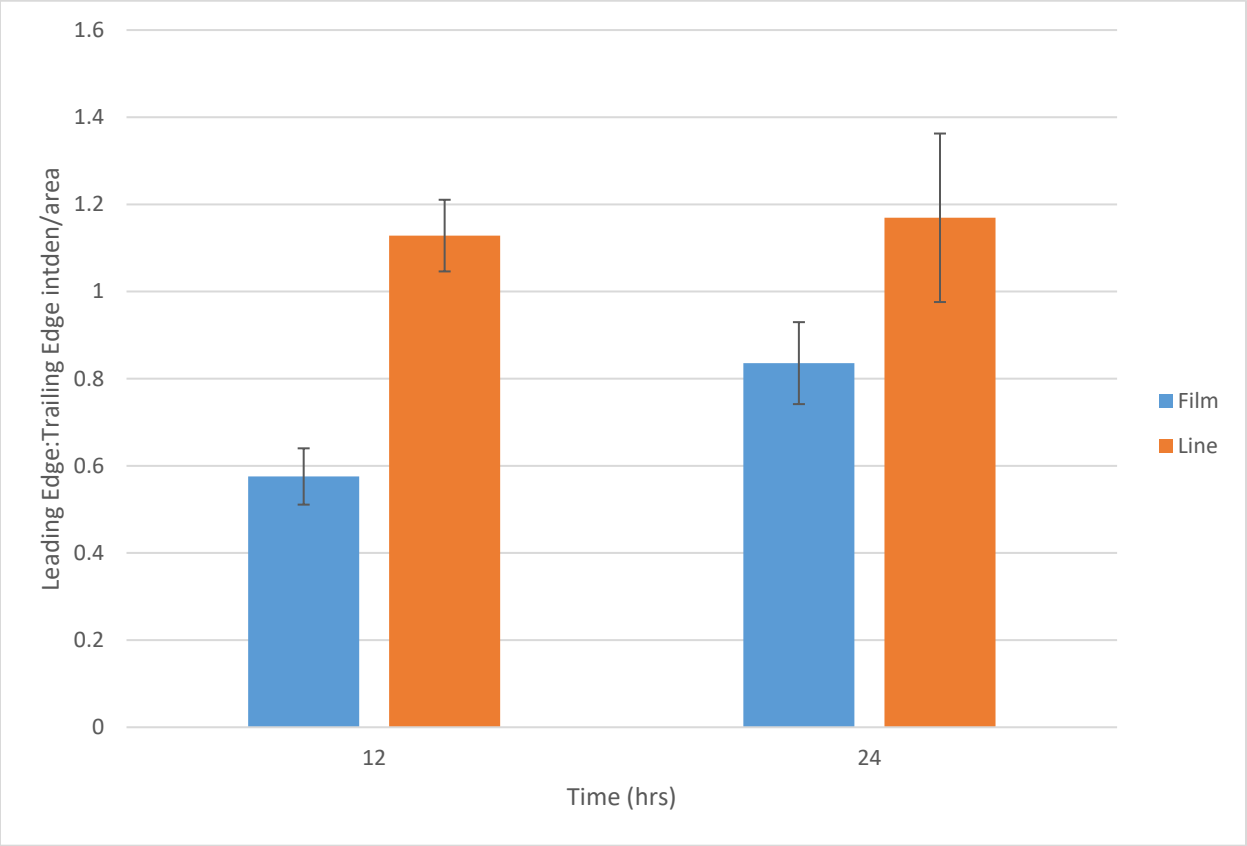

Figure 11. Cells on a line substrate have more NPs at their leading edge than the trailing edge. Cells on a film substrate have more NPs at their trailing edge than their leading edge. The difference between the film and line substrates is statistically significant at 12 hours but not 24 hours. N = 7 and N = 14 for 12 hours on film and line respectively. N = 9 and N = 7 for 24 hours on film and line respectively

Doing an unpaired t-test, the difference between film and line for the 12 hour time point is extremely statistically significant, with a P value of 0.0005. However, for the 24 hour time point, the difference is not statistically significant, having a P value of 0.1026. This may be due to the cells becoming saturated with nanoparticles, which would cause more nanoparticles to be located in a less concentrated region of the cell. This graph also indicates that cells on a film substrate contain more nanoparticles on the trailing edge than on the leading edge and elongated cells on the line substrate have more nanoparticles on the leading edge than on the trailing edge.

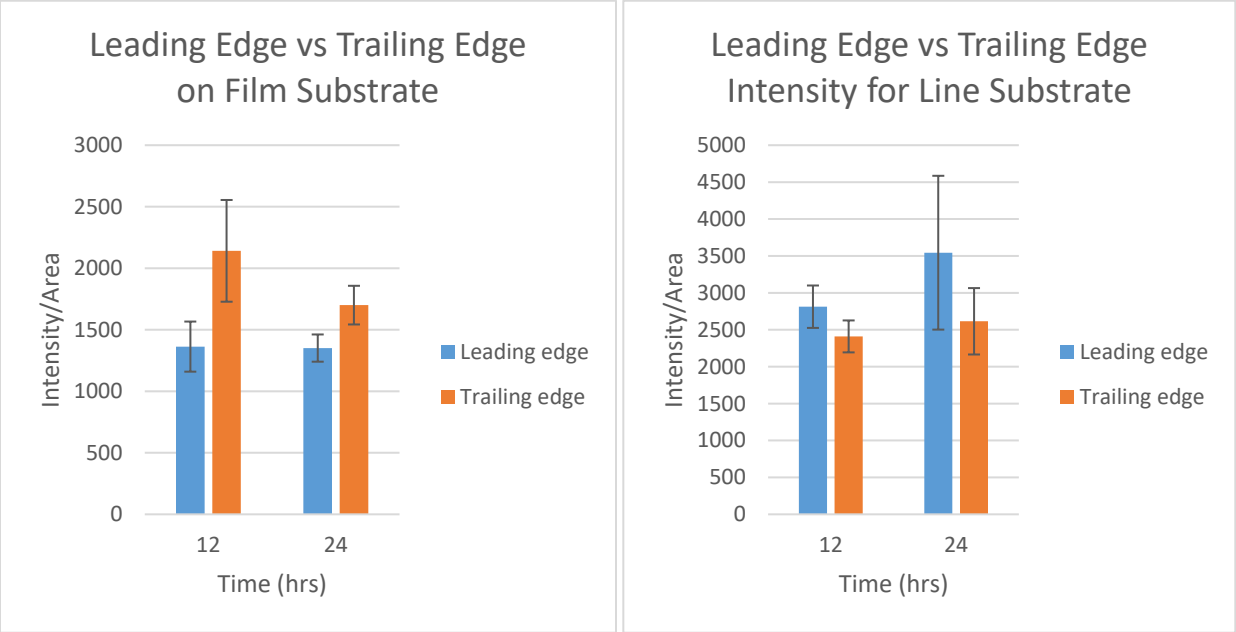

Figure 12. The differences in intensity between the leading edge and trailing edge of cells on both line and film substrates are not statistically significant.

Comparing the leading edge to trailing edge intensities on film and line substrates separately, it can be seen that the cells on the line substrate contain a higher concentration of nanoparticles than the cells on the film substrate. A paired t-test comparing the leading edge concentration to the trailing edge concentration for each substrate and time point showed that there is no statistically significant difference for any time point in either substrate. The P values are 0.1171, 0.2733, 0.0880, 0.4320 for 12 hour film, 12 hour line, 24 hour film, and 24 hour line respectively.

Y-27632 Inhibition

The data from the Y-27632 inhibition experiments suggests that differences in cell tension may not be the only cause of different amounts of nanoparticle intake. By inhibiting the formation of F-actin and myosin II, Y-27632 prevents stress fiber formation. This will severely

dampen any sort of cell contractility and mechanotransduction. The following images show that there is little stress fiber formation in inhibited cells. Images of cells on a film substrate can be seen in Appendix A. The intensity of cells inhibited by Y-27632 was not compared to that of uninhibited cell because this paper is not looking at the effects of drug on nanoparticle uptake.

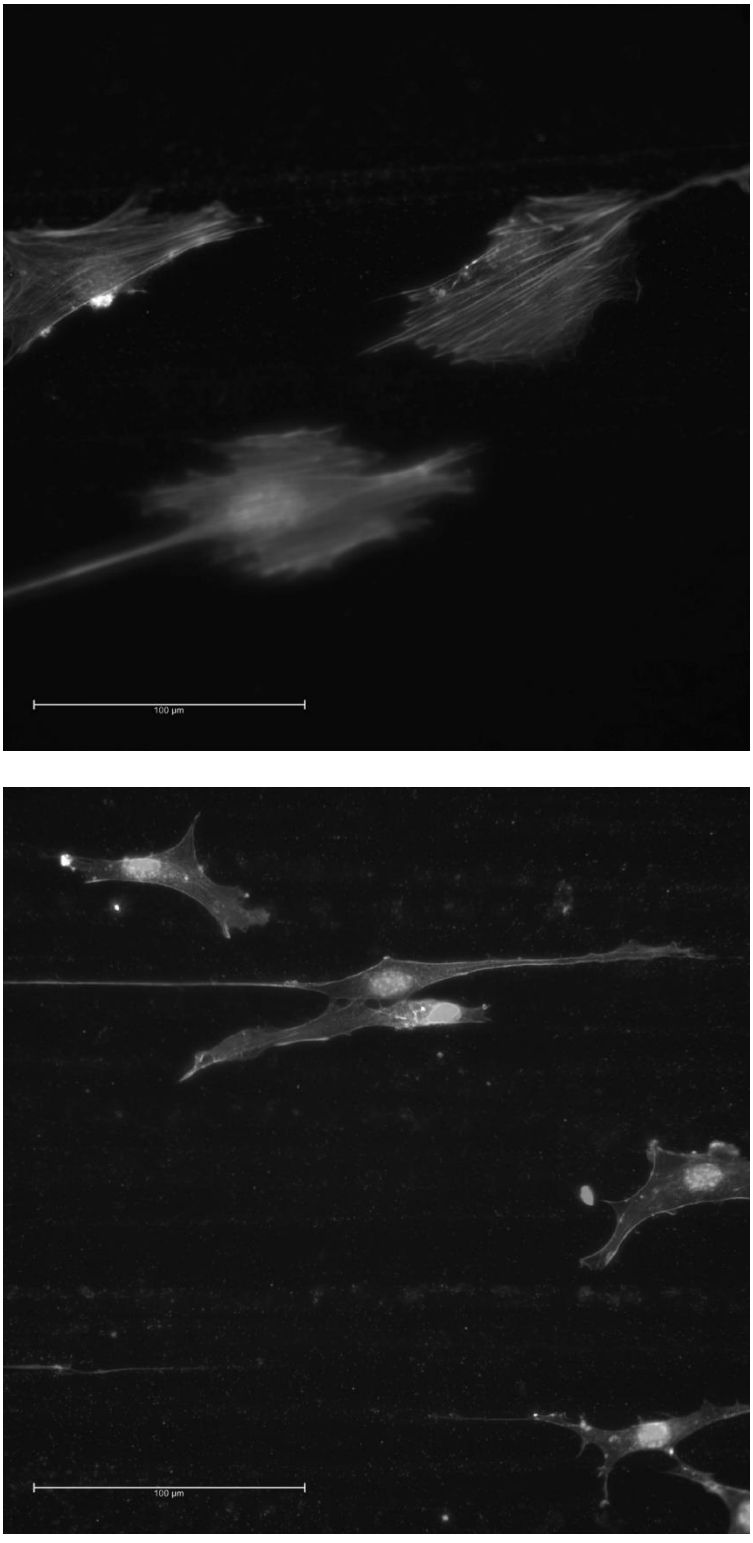

Figure 13. The top image shows MC3T3 cells on a scratched coverslip with no inhibition. The stress fibers can clearly be seen in the cells. The bottom image shows MC3T3 cells on a scratched coverslip with Y-27632 inhibition. Stress fibers cannot be seen

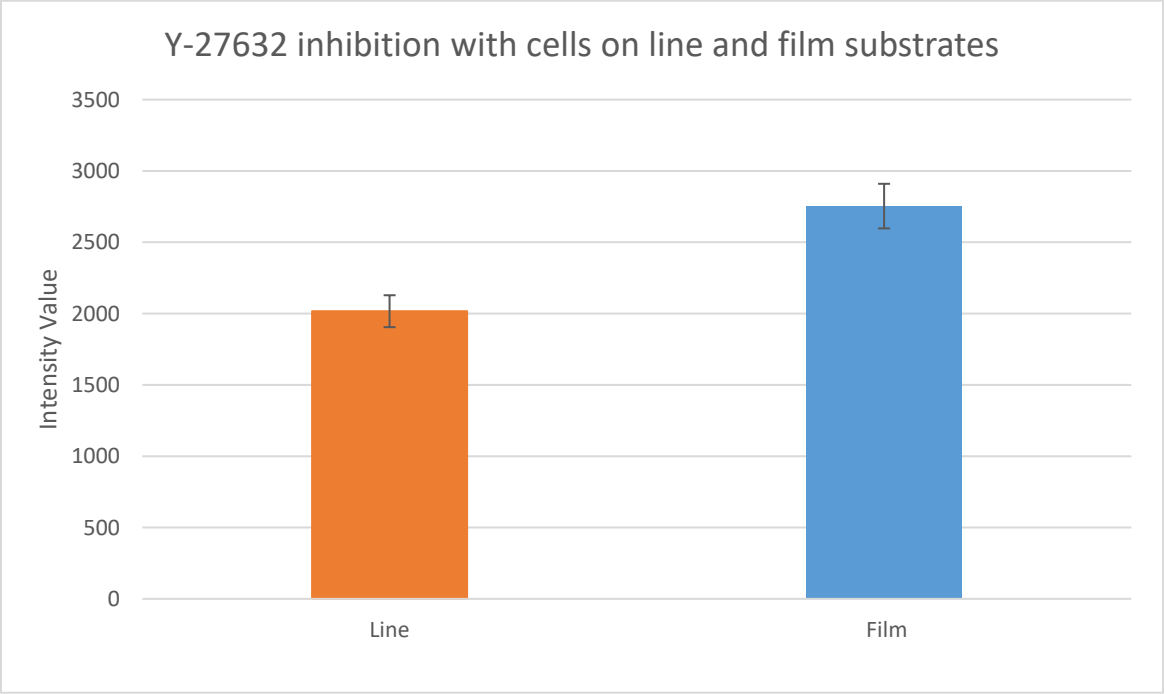

Figure 14. Y-27632 inhibition causes the cells on film to have a higher overall intensity than the cells on line substrate. P = 0.002. N = 52 for line and N = 51 for film

Initially, the data shows that cells on the film substrate consumed more nanoparticles than cells on the line substrate, which is what was observed in the non-inhibition experiment. An unpaired t-test, with N = 52 for the line substrate and N = 51 for film, shows that the results are extremely statistically significant with a P value of 0.002. This indicates that mechanotransduction through the ROCK pathway does not have much influence on the uptake of nanoparticles and that there are other factors at play when it comes to nanoparticle uptake in cells. This also indicates that cell tension may not have as much of an impact on nanoparticle uptake as previously thought.

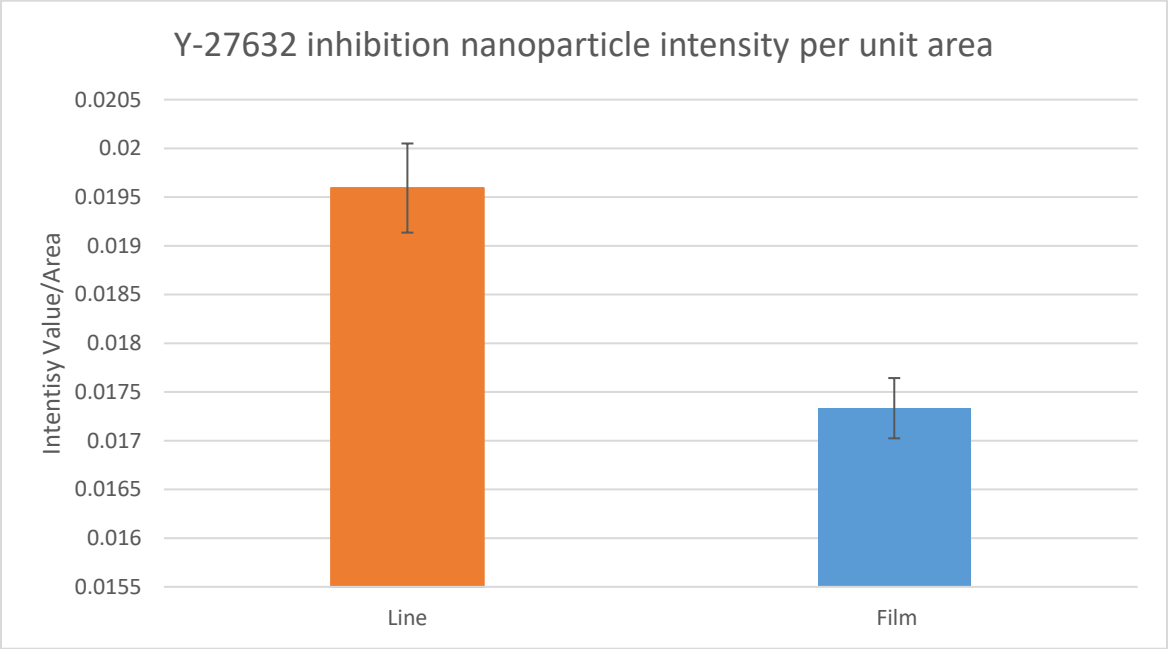

Figure 15. Cells on the line substrate have a higher intensity per unit area than the cells on the film substrate. P = 0.0001

Normalizing the data with respect to area, the trend seen in the non-inhibition study emerges again. The cells on the line substrate have a slightly higher nanoparticle concentration than the cells on the film substrate. An unpaired t-test yields a P value of 0.0001, showing that the difference in nanoparticle uptake between the two substrates is extremely statistically significant.

Microcontact Printing

Microcontact printing was used to control the aspect ratio of the cells. Since it has been shown that a higher cell surface tension results in less nanoparticle uptake and that elongated cells have higher cell surface tension than non-elongated cells, this experiment was intended to show that a higher aspect ratio will intake less nanoparticles. The following images show the

fluorescent nanoparticles within cells of varying aspect ratios. The aspect ratios are increasing going from left to right in each row, from top to bottom.

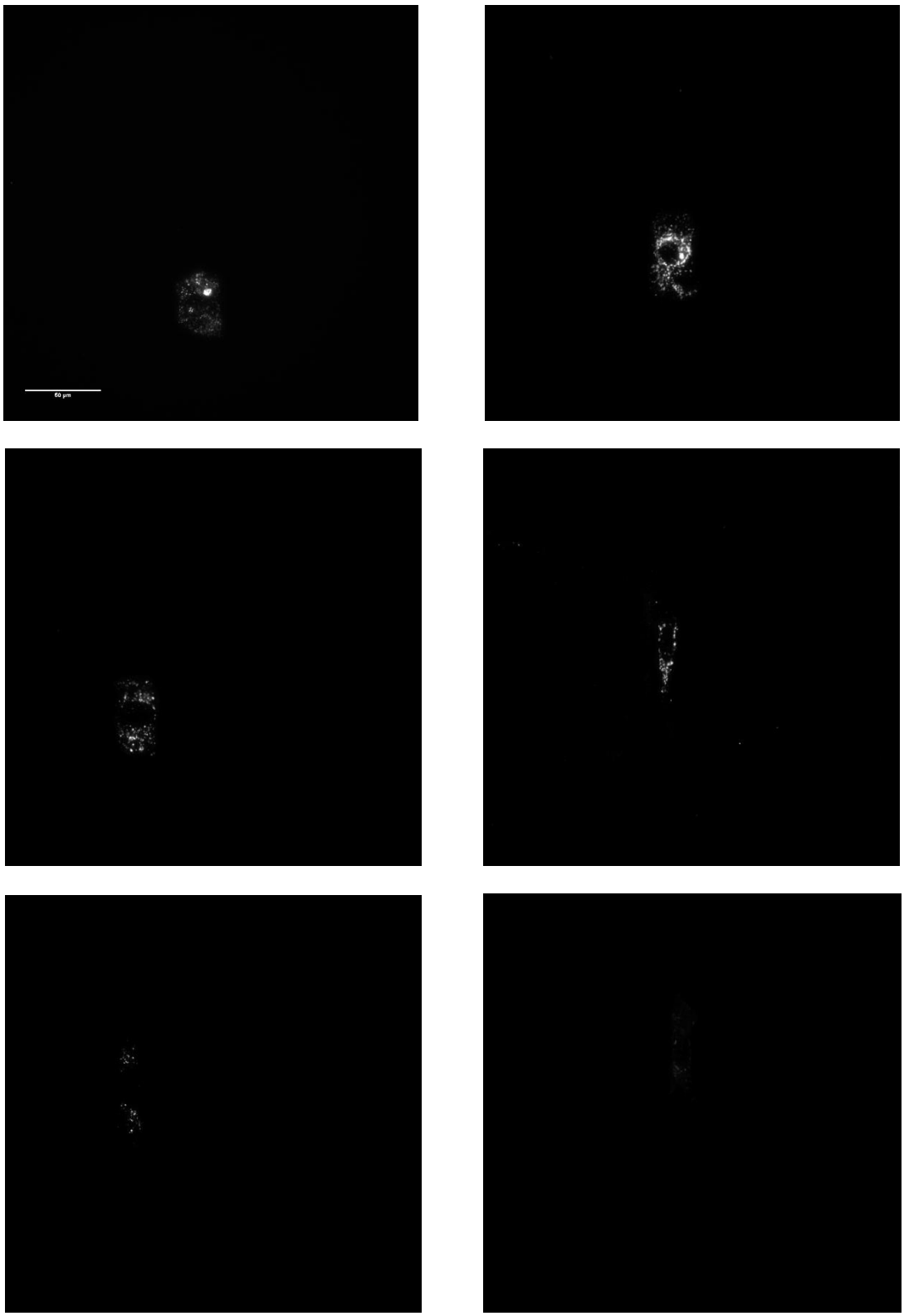

Figure 16. Fluorescent nanoparticles in cells of varying aspect ratios. The scale bar in the top left image is 50 µm. All images were taken at 40x

A purely qualitative analysis shows a general decrease in fluorescence intensity as the aspect ratio increases. While this is only a single series of images, these images indicate the expected outcome of this experiment.

For a quantitative approach, the fluorescence intensity of the nanoparticles was measured. In the first graph below, there is a weak downwards trend in the data. The trend becomes more apparent if the cells are grouped by aspect ratio (1-2 is group one, 2-4 is group two, 4-6 is group three), and the averages are taken of the aspect ratio and intensity/area.

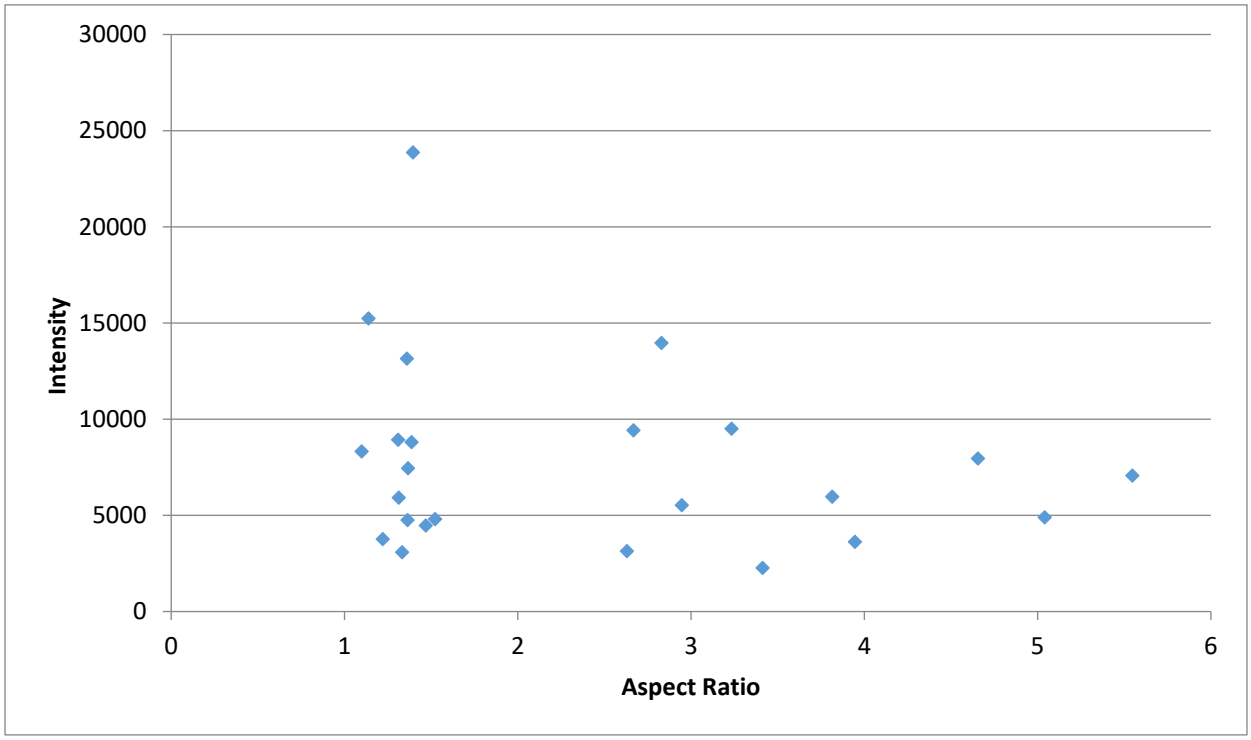

Figure 17. This graph shows a weak downwards correlation between aspect ratio and intensity. N = 25

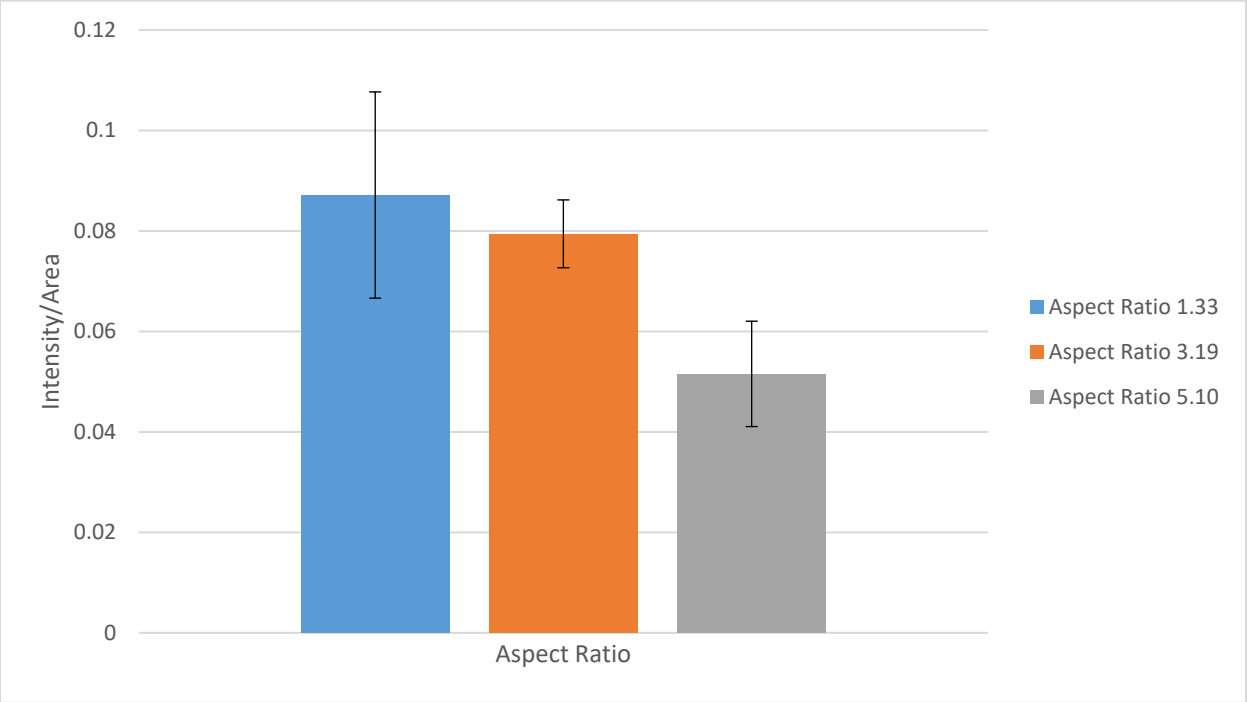

Figure 18. The group one aspect ratio is the average aspect ratio of all cells between 0 - 2. Group two is the average between 2 - 4. Group three is the average between 4 - 6. A larger aspect ratio seems to results in less intensity/area, but there is no statistically significant difference between any of the groups. N = 13 for group one, N = 8 for group two, N = 3 for group three

This trend supports the anticipated outcome of the experiment. It is important to note that it was more difficult to obtain correctly stamped cells at higher aspect ratios than correctly stamped cells at lower aspect ratios; there were only three cells in the 4-6 aspect ratio group, while there were eight cells in the 2-4 group, and 13 cells in the 1-2 group.

Comparing the amount of nanoparticles in the leading edge to that of the trailing edge of cells, it was expected that all cells will have more nanoparticles at the leading edge than at the trailing edge. Additionally, an upwards positive trend was expected so cells with a higher aspect ratio would have a higher ratio of nanoparticles in the leading edge to nanoparticles in the trailing edge.

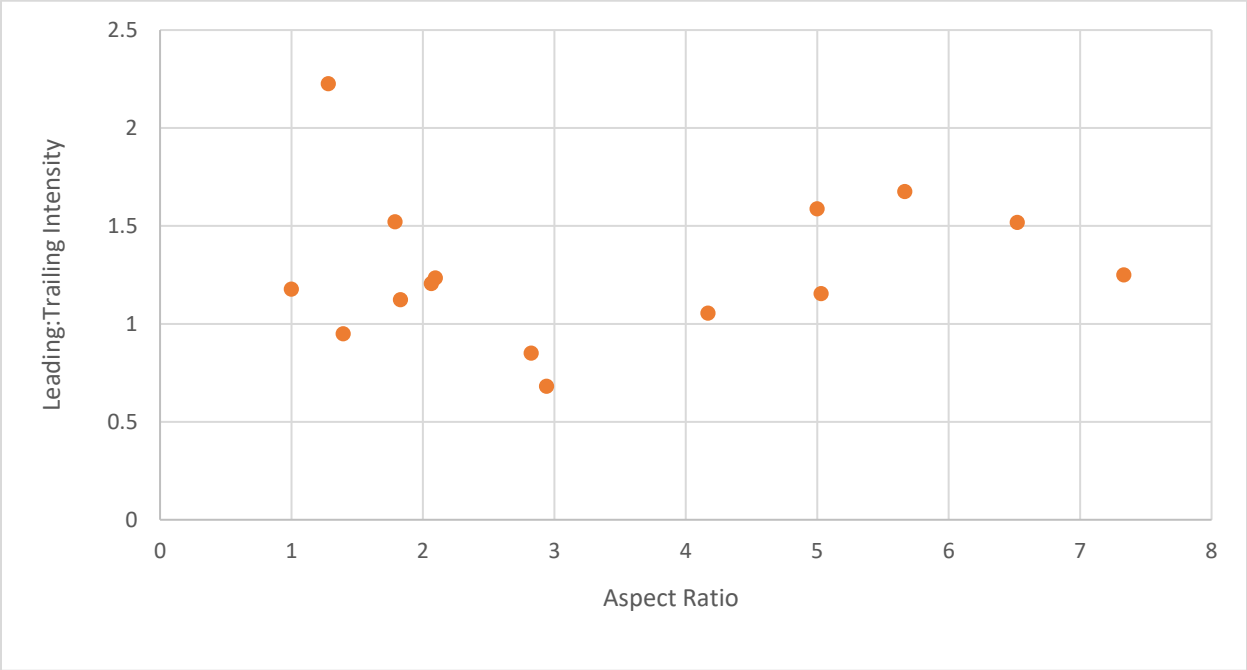

Figure 19. This graph shows no correlation between aspect ratio and leading edge:trailing edge intensity. However, only three cells had more NPs in their trailing edge than their leading edge. N = 15

Looking at the graph, there is no discernable trend in the data. However, it is important to note that out of all fifteen cells measured, only three had more nanoparticles in the trailing edge than in the leading edge. This seems to indicate that the majority of MC3T3 cells will have more nanoparticles in their leading edge than their trailing edge.

Live Cell Imaging

Live cell imaging was done to determine if the nanoparticles are being taken in at the leading edge of the cell as opposed to being transported there via intracellular transport mechanisms. However, the ɣ-tubulin stain used previously in the immunofluorescence experiments could not be used for live cell imaging since the stain requires the cells to be fixed. Thus, the leading edge of the cells could not be identified for this experiment. Despite not identifying the leading edge of cells, this experiment still showed whether the nanoparticles were

being transported within the cell or not. The cell chosen for the time-lapse had an aspect ratio of approximately 3:1.

ImageJ was used to convert multiple images into a stack, and then each image in the stack was assigned a specific color. The first image in each stack is assigned to red and the second image is assigned to green. Overlapping areas are shown in yellow. The first image shows the cell at the initial time-point and at 15 minutes. This image indicates that nanoparticle movement is occurring within the cell since the image is not entirely yellow. Transport from the top to the bottom of the cell can be seen on the right side of the cell.

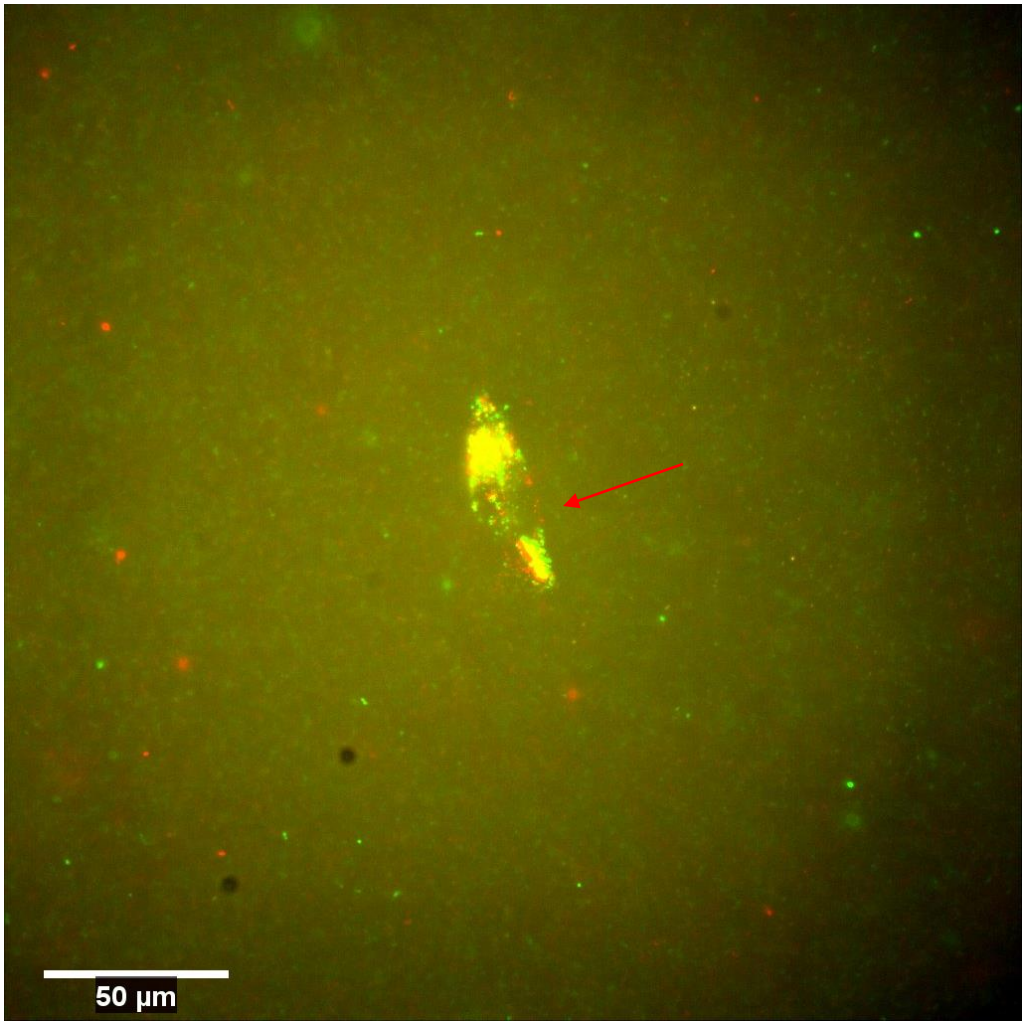

Figure 20. Times 0 and 15 minutes of the time-lapse. The first image is shown in red while the second image is shown in green. Overlapping areas are shown in yellow

The second image shows the nanoparticles at times 15 minutes and 30 minutes. What was green in the first picture is now red in the second picture. A more definitive example of nanoparticle transport from the top to the bottom of the cell can be seen here and in the third picture at the left side of the cell.

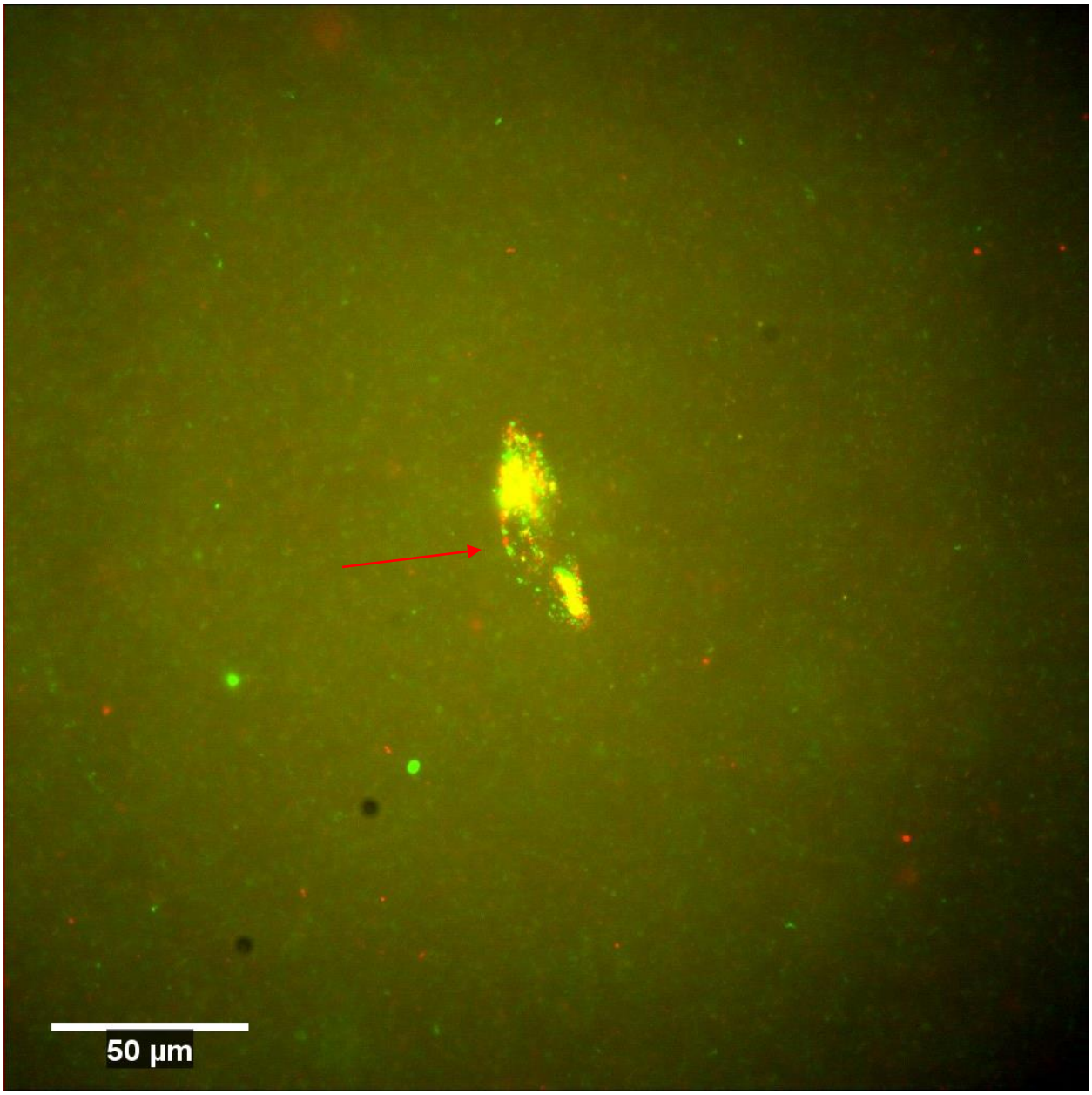

Figure 21. Images at 15 and 30 minutes into the time-lapse. The image at 15 minutes is in red and 30 minutes is in green

The third picture shows a continuation of this nanoparticle transport from 30 minutes to 45 minutes. As previously stated, the green image in the second picture is now red in the third picture.

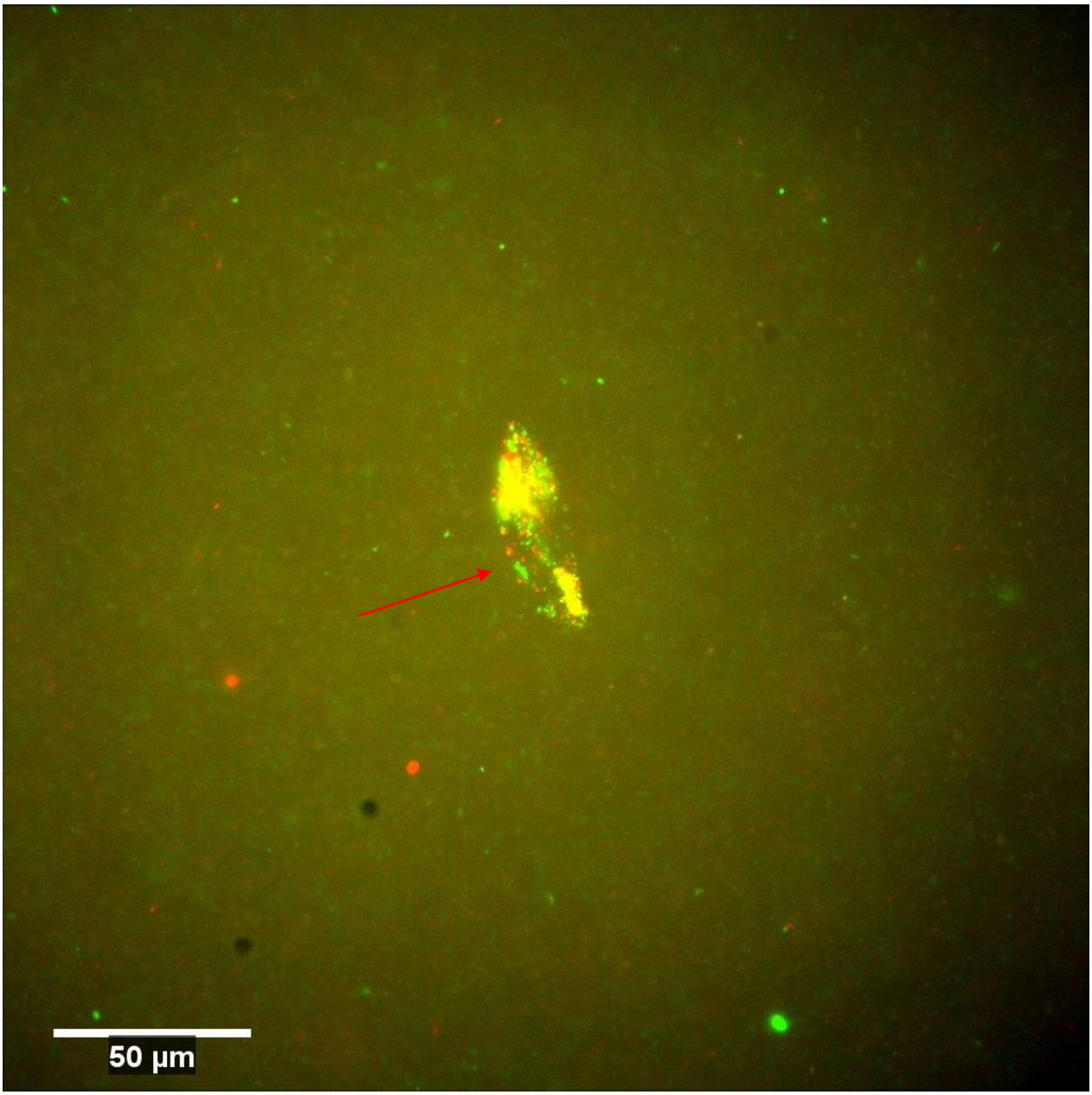

Figure 22. Images at 30 and 45 minutes into the time-lapse. 30 minutes is in red and 45 minutes is in green

These pictures indicate that nanoparticle transport is occurring and the nanoparticles are moving from the top of the cell to the bottom of the cell. However, since the ɣ-tubulin stain

could not be used, it is unclear whether the top or bottom half is the leading edge. While an educated guess could be made by measuring the intensities to see which side has more nanoparticles, the images from the live-cell experiments are overexposed so data is lost from the image.

A qualitative analysis can still be made on the resulting images. At the initial time point shown below, there are nanoparticles at either end of the cell; there are very few in the center of the cell. The top half appears to have more nanoparticles than the bottom half at this time.

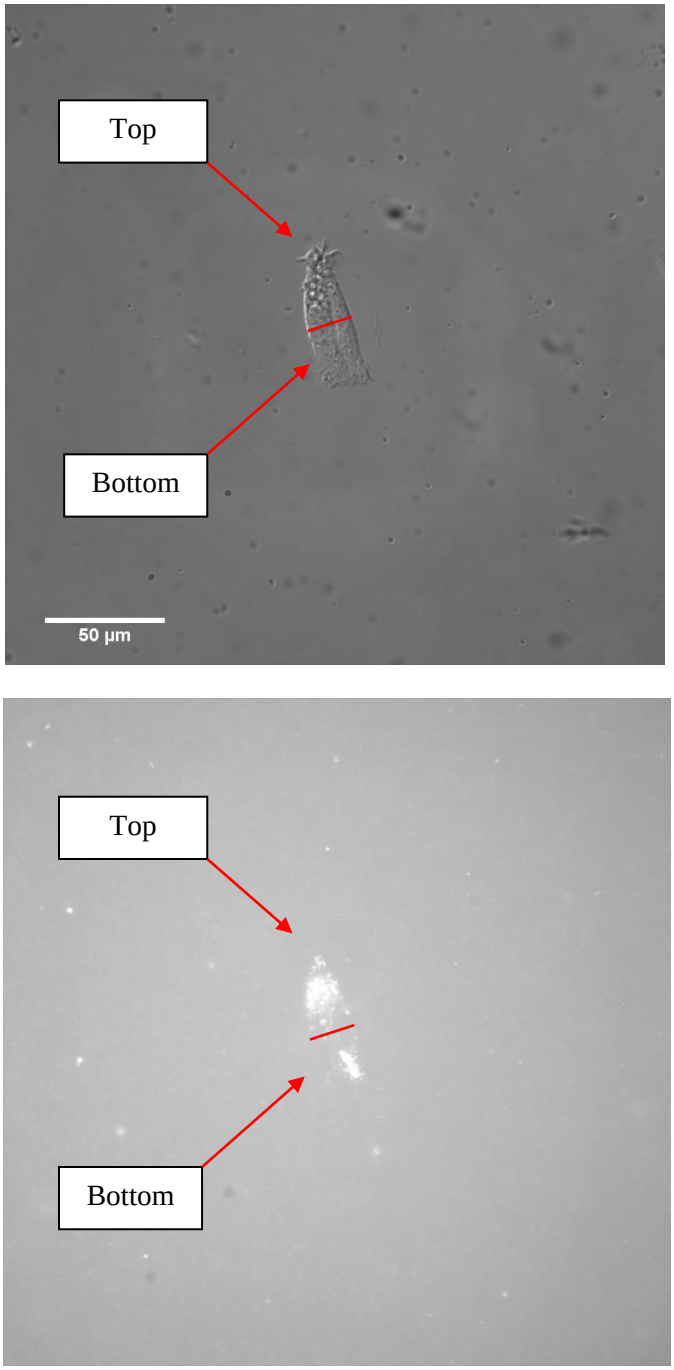

Figure 23. Time zero of the time-lapse. The top image shows the DIC image while the bottom image shows the fluorescent image

One hour into the time-lapse, it looks like both the top half and bottom half have increased in intensity. The top half of the cell still appears to have more nanoparticles than the bottom half.

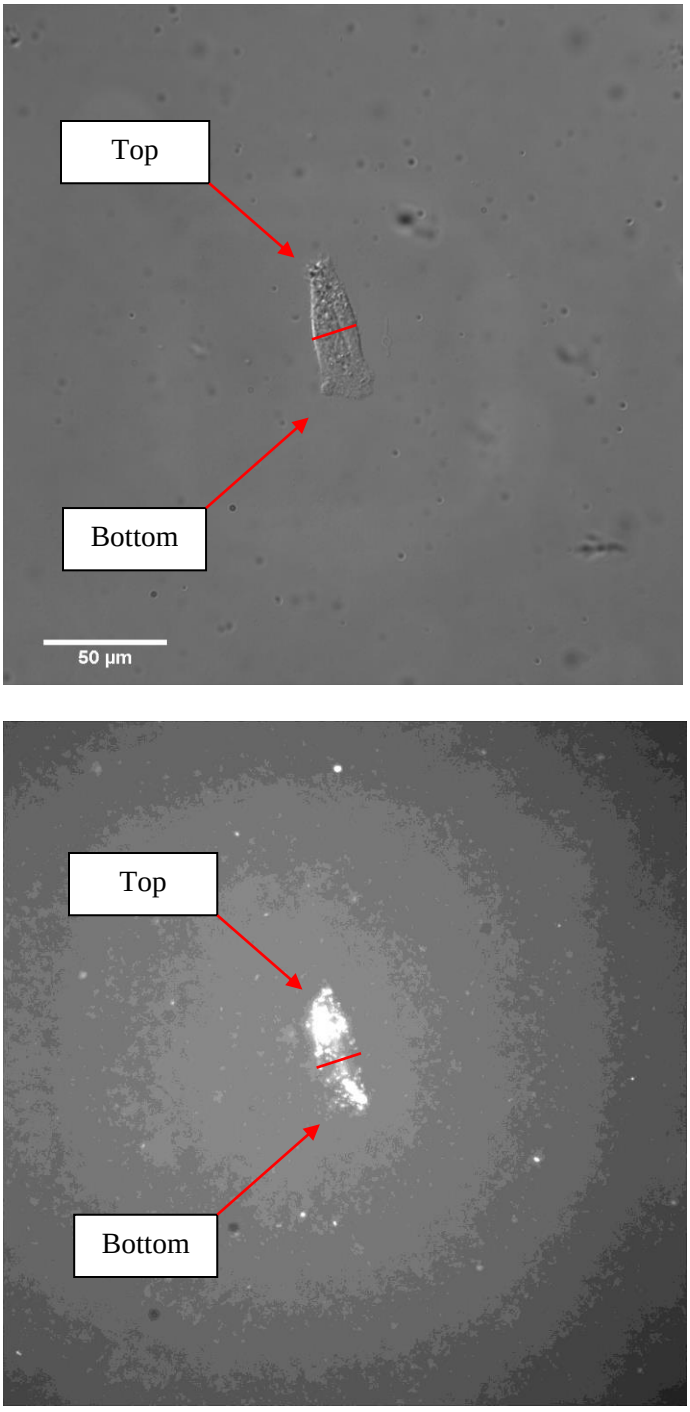

Figure 24. 100 minutes into the time-lapse

Five hours into the time-lapse, both ends seem to have increased in intensity again. This observation correlates with previous experiments, as well as intuition, that show that cells will intake more nanoparticles when they are exposed to nanoparticles for a longer period of time.

However, at the five hour point, the bottom half of the cell appears to have a higher intensity than the top half. Whether this is due to a higher intake rate at the bottom half, intracellular transport, or a combination of the two is unknown. At eight hours, the microscope began to shift out of focus, so any images from this point on will not be an accurate representation of the nanoparticles in the cell.

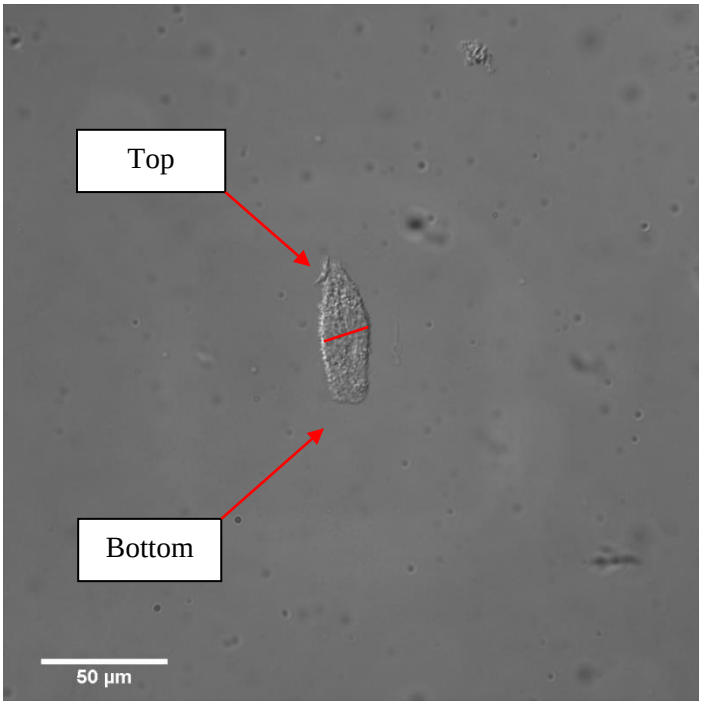

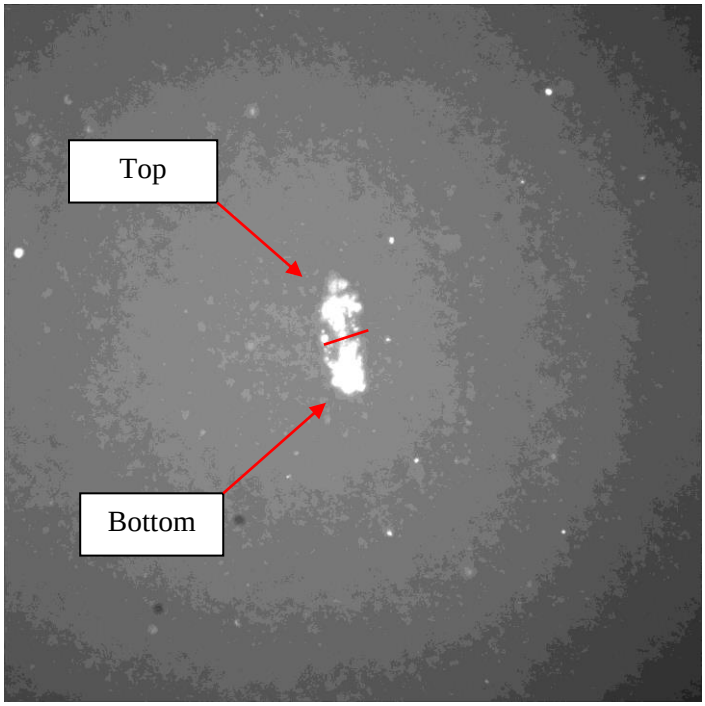

Figure 25. Five hours into the time-lapse

A second live-cell imaging experiment was completed. However, during the experiment, a large aggregate of nanoparticles gets caught on the cell. It was unclear whether the

nanoparticles were absorbed into the cell or not. Half of the cell also detached from the slide within three hours of initiating the time-lapse. Images from this time-lapse can be seen in the appendix.

Chapter 4

Conclusions and Future Directions

The work shown here indicates a difference in uptake in non-elongated cells and elongated cells as well as uptake at the leading edge and trailing edge of cells. These results are most clearly seen in the film vs line and microcontact printing experiments. While these experiments have illustrated some of the patterns behind nanoparticle uptake in MC3T3 cells, there is still much to learn and improve upon. One issue that still requires clarification is nanoparticle transport within the cell. Since the cell stamping experiment has shown that a majority of MC3T3 cells have more nanoparticles at the leading edge than at the trailing edge regardless of aspect ratio, it is important to understand how the nanoparticles arrived at the leading edge. Upon cell entry, nanoparticles can be transported within the cell via actin filaments and motor proteins. Thus, nanoparticles may be being transported to the leading edge as opposed to being endocytosed at the leading edge. While the live-cell imaging showed that nanoparticles were moving from one end of the cell to the other, it was unclear which edge was the leading edge. An experiment can be done in which motor proteins are inhibited to see if nanoparticles are being taken in at an increased rate at the leading edge rather than being transported there. The inhibitors will stop intracellular transport so the nanoparticles will not

move after entering the cell. This experiment can use the γ-tubulin stain utilized in the coverslip and microcontact printing experiments.

While cell stamping provided a way to control cell elongation, it also prevented natural cell movement. By confining cells to the stamped shapes, they could not migrate or move as they would *in vivo*. This could affect endocytosis pathways since cell migration and endocytosis are closely linked. Near-field electrospinning could be utilized to create an organized extracellular matrix-like structure that promotes cellular elongation[24]. Although cellular elongation cannot be as strictly controlled with this method as with microcontact printing, it would allow for cell migration while providing more elongation control than using a scratched coverslip.

As previously stated, the images from the live-cell experiment were overexposed. This experiment would have to be repeated to obtain accurate data before conclusions can be drawn. Another live-cell imaging experiment that could be done would be to image and compare nanoparticle uptake in less elongated cells to that in more elongated cells. This can also be used to observe intracellular transport mechanisms to see if they differ between elongated and non-elongated cells.

The end goal of this research would be to discover the specific mechanisms behind nanoparticle uptake and how they are affected by mechanotransduction. This would have to be done via various biological assays. While this goal is currently unmet, progress is quickly being made to reach it. Upon completion, the knowledge attained would greatly aid in the development of pharmaceuticals and nanomedicines.

Appendix A

Y-27632 Inhibition on Film Substrate

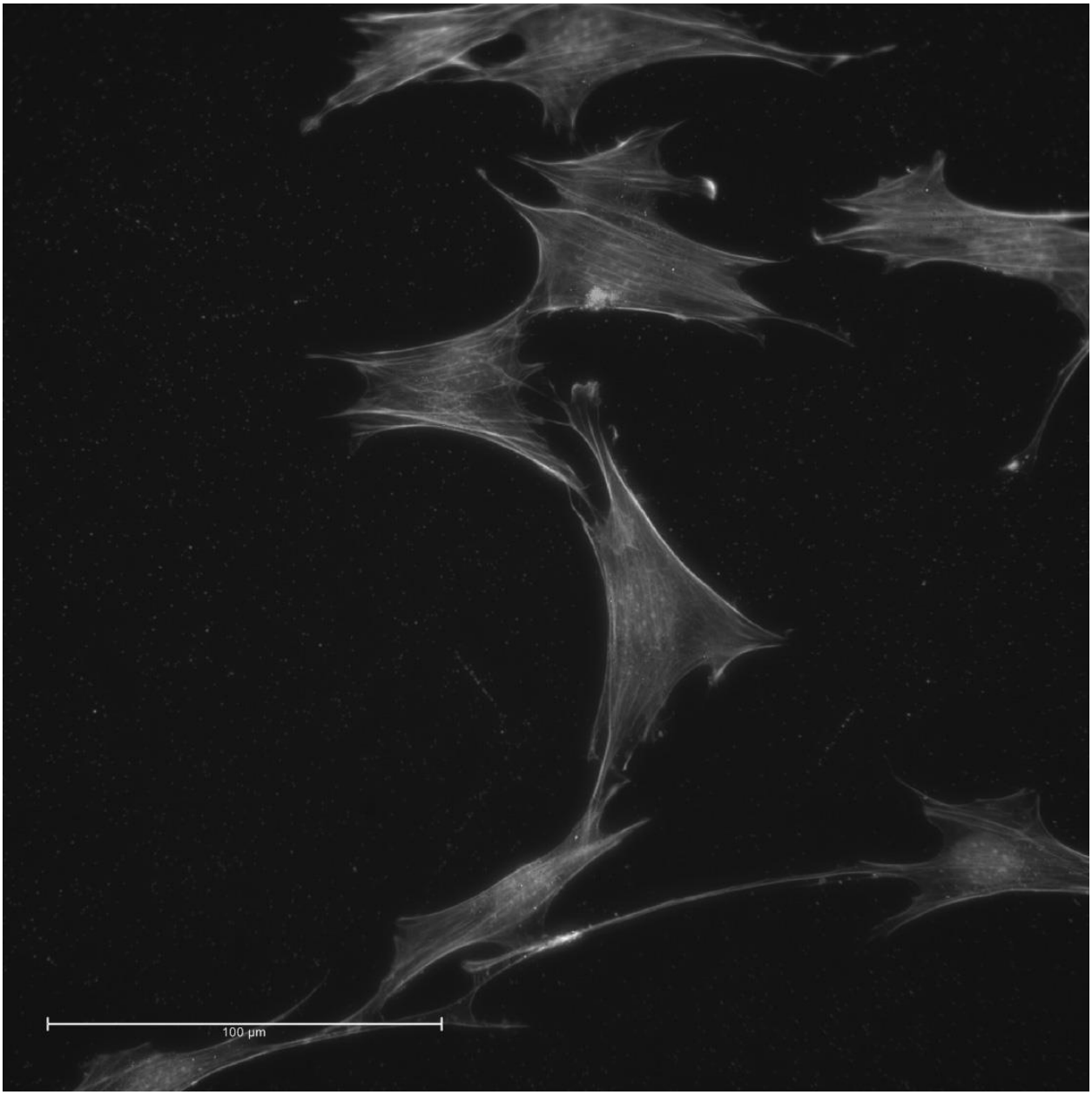

Figure 26. MC3T3 cells on a film substrate with no inhibition. Stress fibers can be seen in the cells

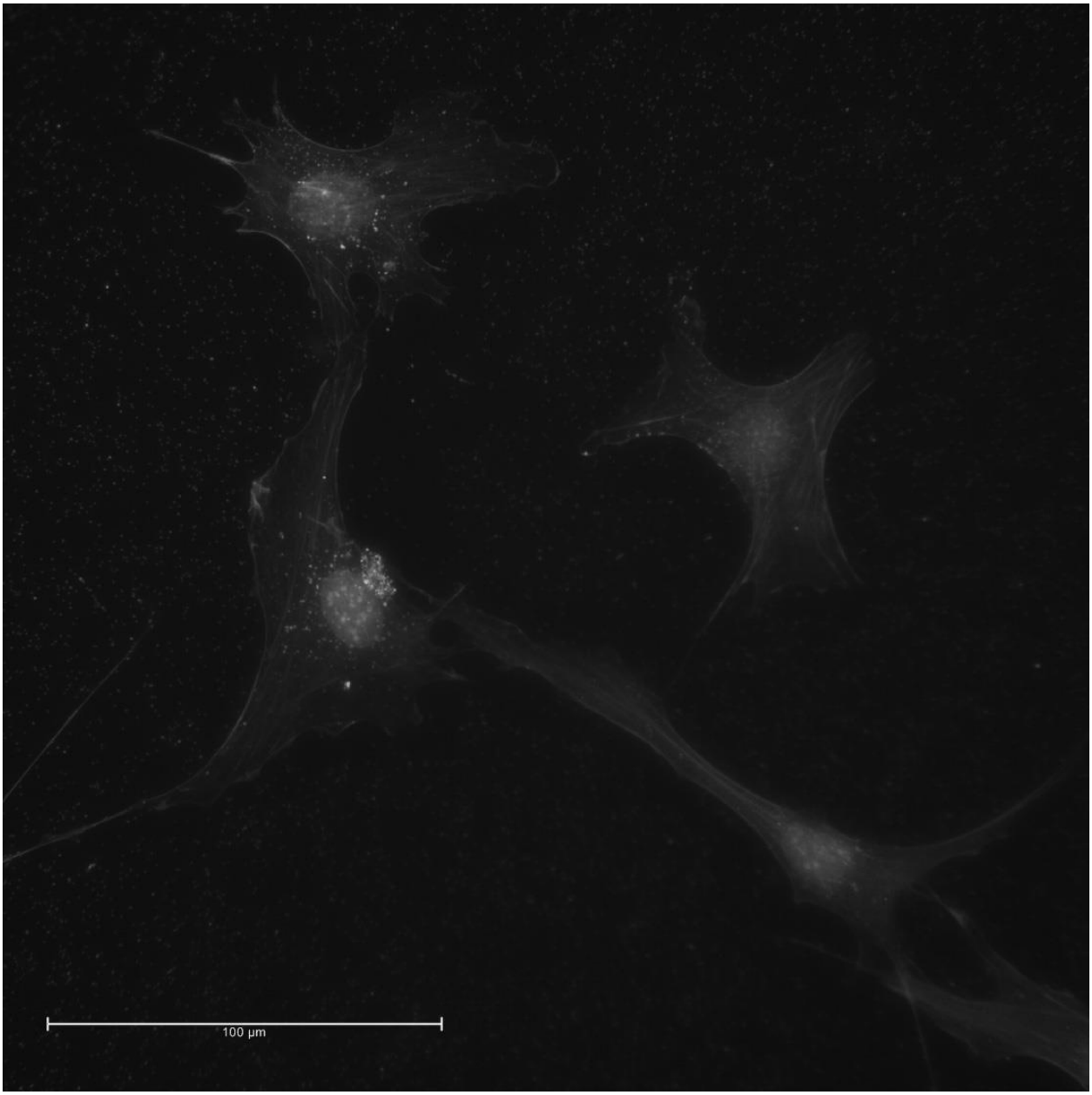

Figure 27. MC3T3 cells on a film substrate with Y-27632 inhibition. Stress fibers cannot be seen in the cells

Appendix B

Live-Cell Imaging Experiment II

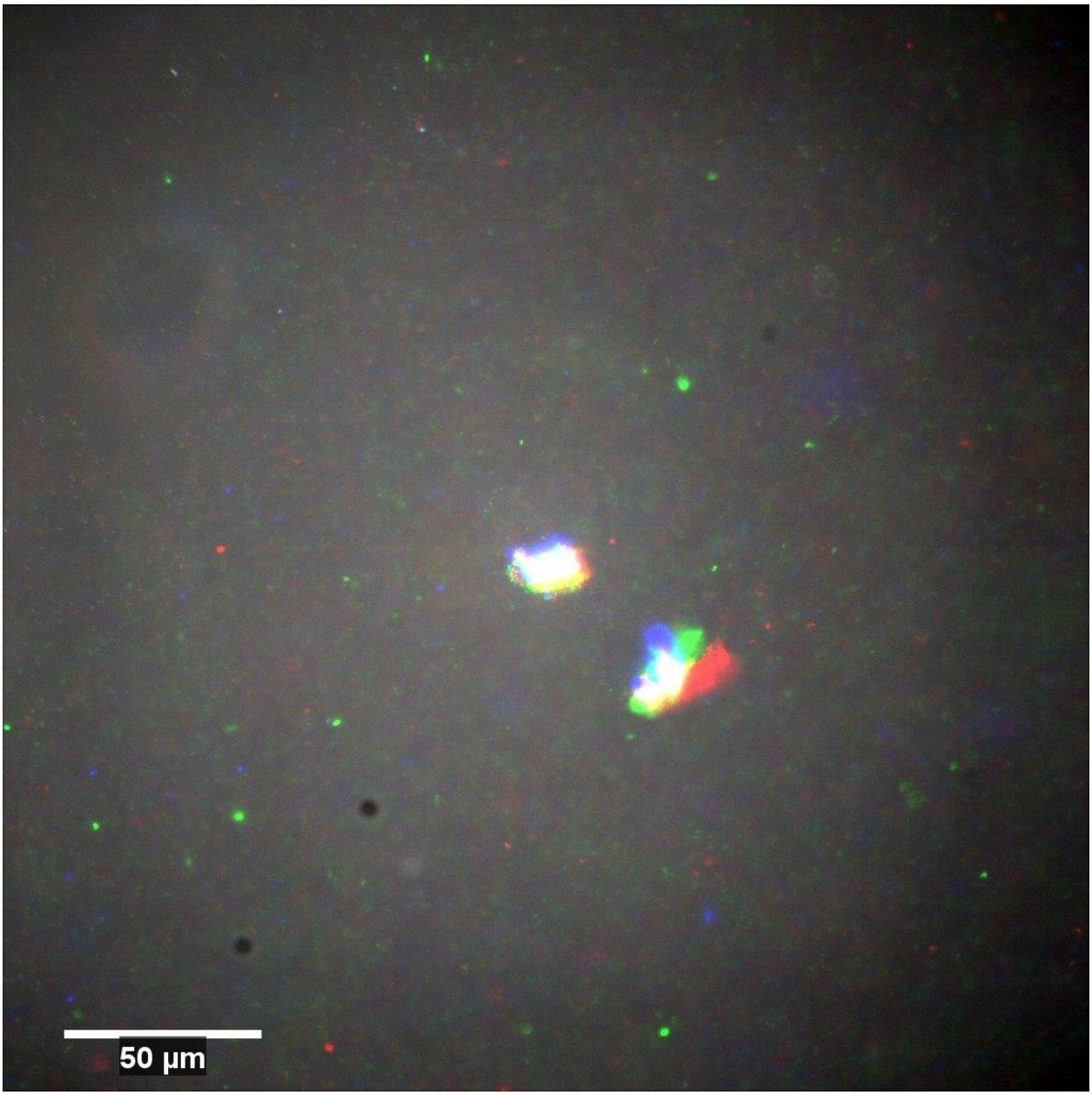

Figure 28. Nanoparticle movement in the cell at 80 minutes (red), 90 minutes (green), and 100 minutes (blue)

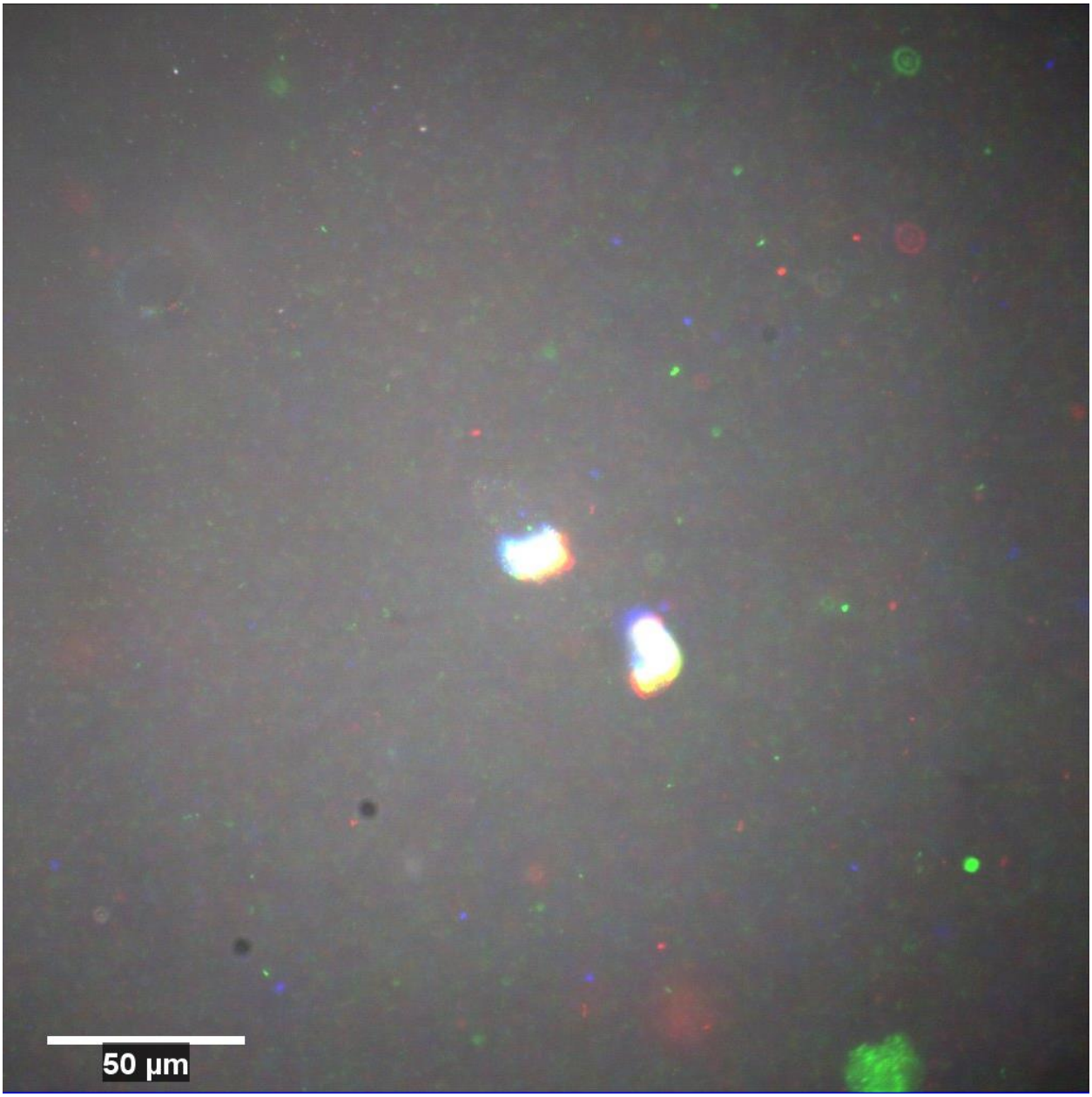

Figure 29. Nanoparticle movement in the cell at 115 minutes (red), 125 minutes (green), and 135 minutes (blue)

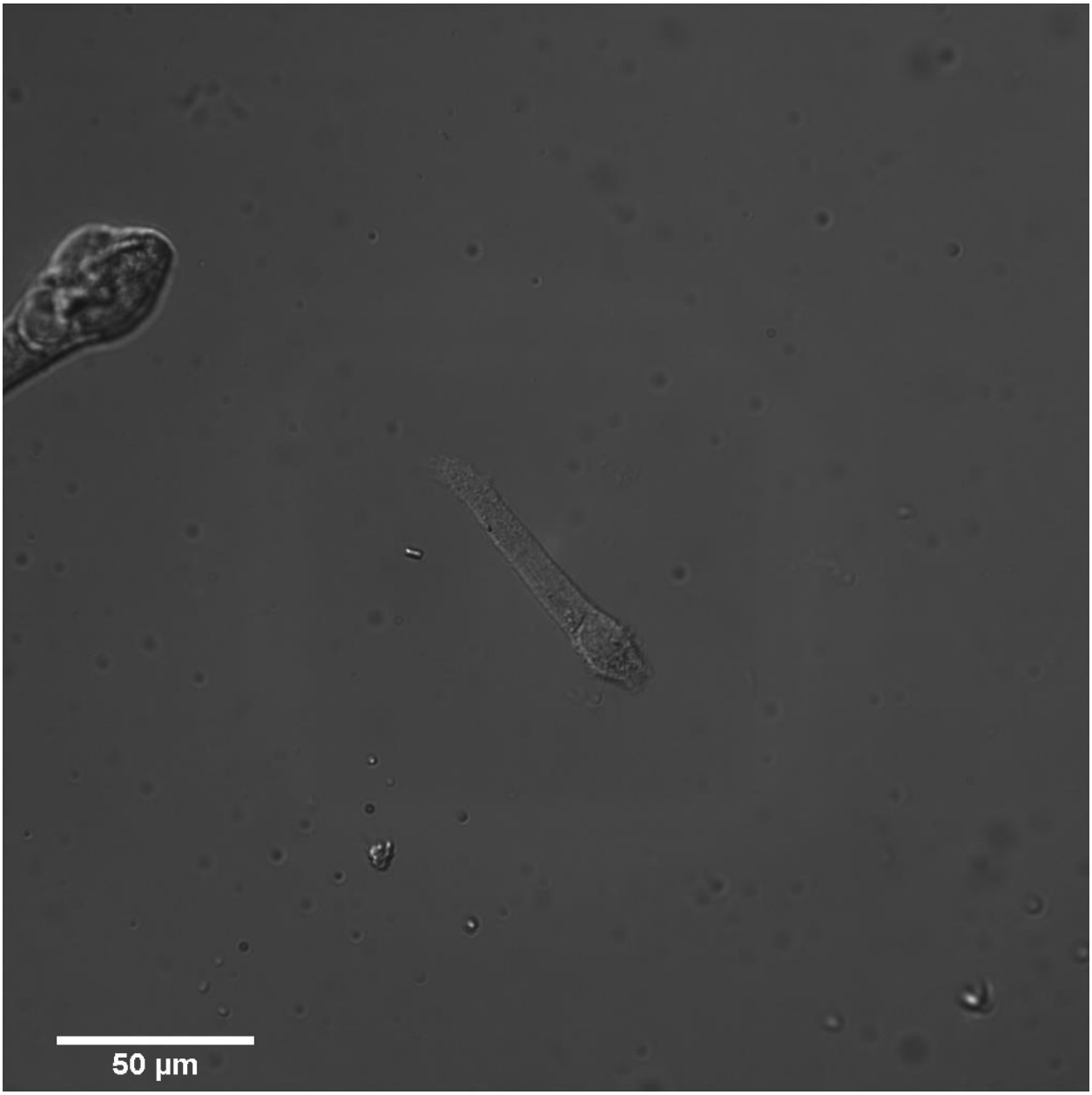

Figure 30. DIC image of the cell at time zero

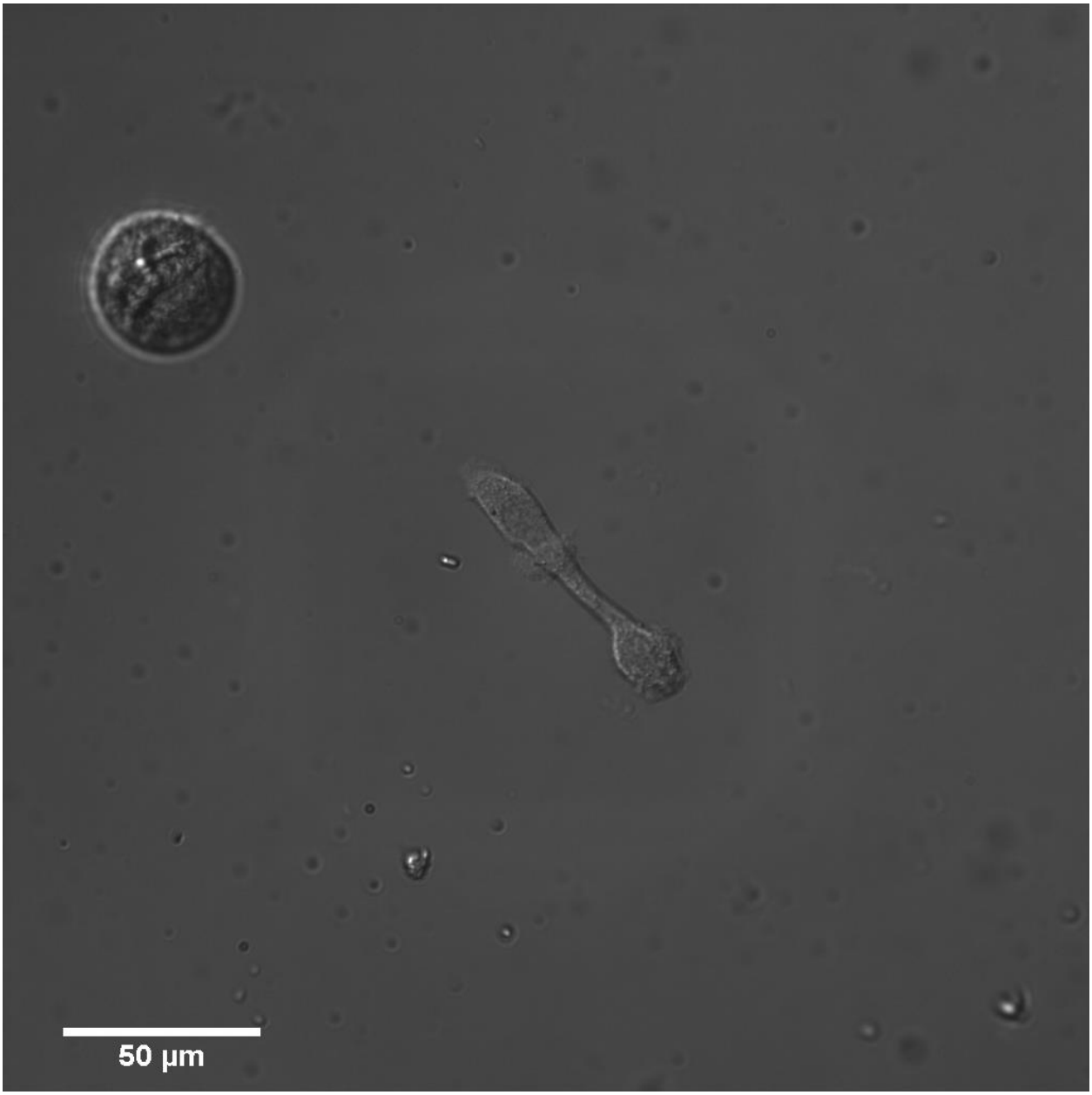

Figure 31. DIC image of the cell at 100 minutes

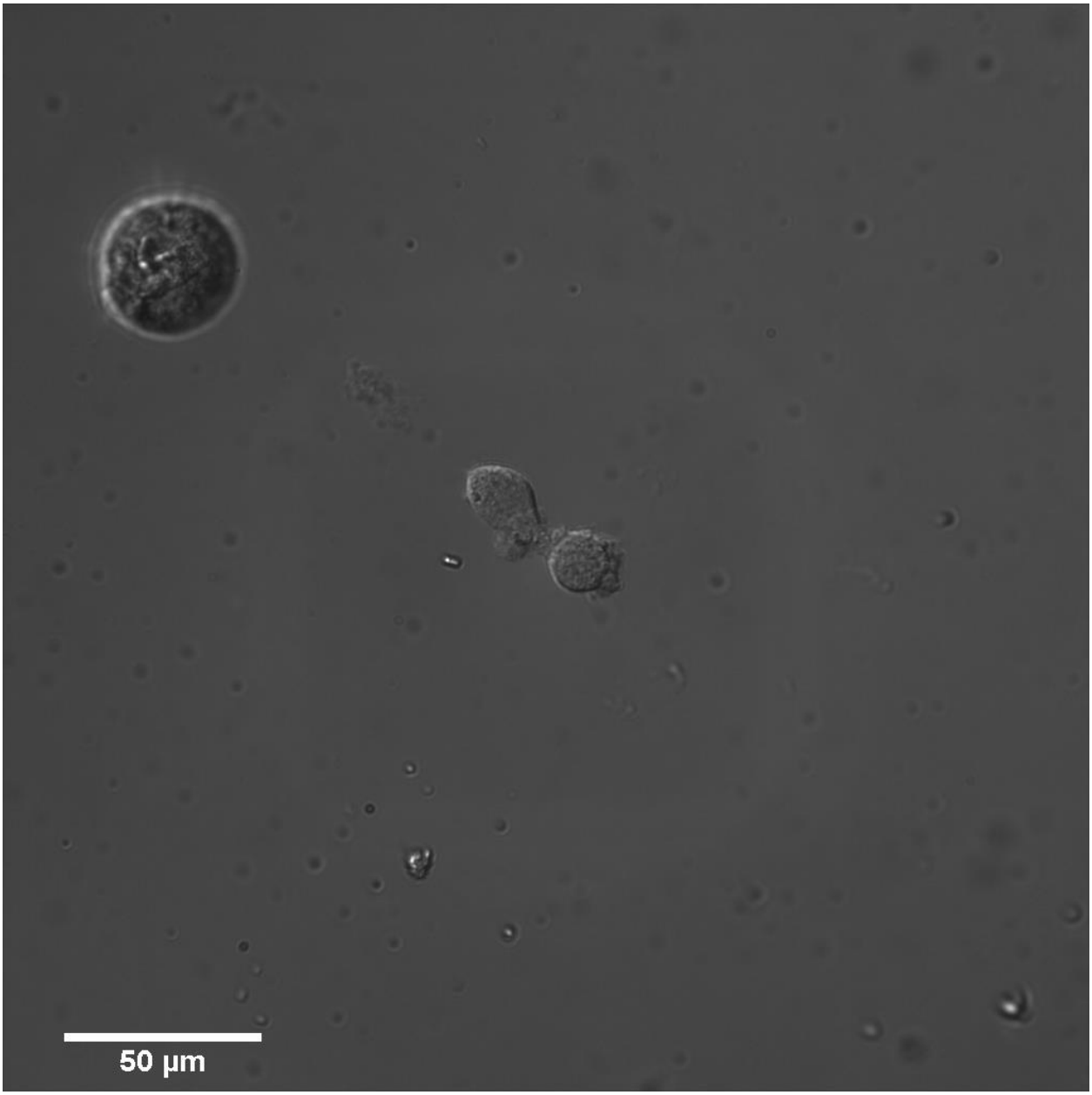

Figure 32. DIC image of the cell at 160 minutes

BIBLIOGRAPHY

1. Davis, M. E., Chen, Z. G. & Shin, D. M. Nanoparticle therapeutics: an emerging treatment modality for cancer. *Nat. Rev. Drug Discov.* **7,** 771–782 (2008).
2. Rosen, H. & Abribat, T. The rise and rise of drug delivery. *Nat. Rev. Drug Discov.* **4,** 381–385 (2005).
3. Park, K. Controlled drug delivery systems: Past forward and future back. *J. Control. Release* **190,** 3–8 (2014).
4. Hoffman, A. S. The origins and evolution of 'controlled' drug delivery systems. *J. Control. Release* **132,** 153–163 (2008).
5. Birrenbach, G. & Speiser, P. P. Polymerized Micelles and Their Use as Adjuvants in Immunology. *J. Pharm. Sci.* **65,** 1763–1766 (1976).
6. Kreuter, J. & Speiser, P. P. In Vitro Studies of Poly(methyl Methacrylate) Adjuvants. *J. Pharm. Sci.* **65,** 1624–1627 (1976).
7. Banik, B. L., Fattahi, P. & Brown, J. L. Polymeric nanoparticles: The future of nanomedicine. *Wiley Interdiscip. Rev. Nanomedicine Nanobiotechnology* **8,** 271–299 (2016).
8. Kulkarni, S. a & Feng, S.-S. Effects of particle size and surface modification on cellular uptake and biodistribution of polymeric nanoparticles for drug delivery. *Pharm. Res.* **30,** 2512–22 (2013).
9. Sahay, G., Alakhova, D. Y. & Kabanov, A. V. Endocytosis of nanomedicines. *J. Control.*

Release **145,** 182–195 (2010).

10. He, C., Hu, Y., Yin, L., Tang, C. & Yin, C. Effects of particle size and surface charge on cellular uptake and biodistribution of polymeric nanoparticles. *Biomaterials* **31,** 3657–3666 (2010).
11. Hyeon, T. & Rotello, V. Nanomedicine themed issue and therapy w. *Chem. Soc. Rev.* **41,** 2545–2561 (2012).
12. Farokhzad, O. C. & Langer, R. Nanomedicine: Developing smarter therapeutic and diagnostic modalities. *Adv. Drug Deliv. Rev.* **58,** 1456–1459 (2006).
13. Voigt, J., Christensen, J. & Shastri, V. P. Differential uptake of nanoparticles by endothelial cells through polyelectrolytes with affinity for caveolae. *Proc. Natl. Acad. Sci. U. S. A.* **111,** 2942–7 (2014).
14. Conner, S. D. & Schmid, S. L. Regulated portals of enrty into the cell. *Nature* **422,** 37–43 (2003).
15. Kumari, S., Mg, S. & Mayor, S. Endocytosis unplugged: multiple ways to enter the cell. *Cell Res.* **20,** 256–275 (2010).
16. Oh, P. *et al.* Live dynamic imaging of caveolae pumping targeted antibody rapidly and specifically across endothelium in the lung. *Nat. Biotechnol.* **25,** 327–337 (2007).
17. Mayor, S. & Pagano, R. E. Pathways of clathrin-independent endocytosis. *Nat. Rev. Mol. Cell Biol.* **8,** 603–612 (2007).
18. Huang, C. *et al.* The role of substrate topography on the cellular uptake of nanoparticles. *J. Biomed. Mater. Res. - Part B Appl. Biomater.* **104,** 488–495 (2016).
19. Huang, C. *et al.* Substrate stiffness regulates cellular uptake of nanoparticles. *Nano Lett.* **13,** 1611–1615 (2013).

20. Fattahi, P., Butler, P. J. & Brown, J. L. Nano Letters,. **5,** 2013 (2014).

21. Huang, S. & Ingber, D. E. Cell tension, matrix mechanics, and cancer development. *Cancer Cell* **8,** 175–176 (2005).

22. Lin, H. C. *et al.* Quantitative measurement of nano-/microparticle endocytosis by cell mass spectrometry. *Angew. Chemie - Int. Ed.* **49,** 3460–3464 (2010).

23. Chithrani, B. D., Ghazani, A. A. & Chan, W. C. W. Determing the Size and Shape Dependence of Gold Nanoparticles Uptake Into Mammalian Cells. *Nano Lett.* **6,** 662–668 (2006).

24. He, X. X. *et al.* Near-Field Electrospinning: Progress and Applications. *J. Phys. Chem. C* **121,** 8663–8678 (2017).

25. Champion, J. a, Katare, Y. K. & Mitragotri, S. Making polymeric micro- and nanoparticles of complex shapes. *Proc. Natl. Acad. Sci. U. S. A.* **104,** 11901–4 (2007).